Самозахват мощных лазерных импульсов и ядерная фотоника

В. Ю. Быченков

Физический институт им. П. Н. Лебедева РАН, Москва
Центр фундаментальных и прикладных исследований(ЦФПИ), ВНИИА, РОСАТОМ, Москва

XIX НАУЧНАЯ ШКОЛА
“Нелинейные волны -2020”

29 февраля - 6 марта 2020 г.

Contributors

recent (2018-2020) advances in relativistic nonlinear optics for applications

Lebedev Physics Institute & CFAR, VNIIA, ROSATOM, Russia :

A. V. Brantov, M. G. Lobok, V. F. Kovalev, O. E. Vais

Weizmann Institute of Science, Israel :

I.A. Andriyash, V. Malka

Outline

I. Relativistic intense soliton in the service of nuclear photonics:

- **Acceleration of electrons from low-density targets n_e ~< n_c for maximization of total electron charge.**
- **Self-trapping regime. The matched beam spot size to density condition. Laser bullet (soliton).**
- **Production of gammas and pairs. Deep gamma-radiography.**
- **Production of neutrons and photonuclear elementary particles.**
- **Isotope production**

II. New laser-based THz-sources:

- **Ultrafast target charging by laser-accelerated electrons.**
- **THz surface wave.**

III. How to measure relativistic intense laser pulse:

Historical excursion

Volume 13, Number 15 PHYSICAL REVIEW LETTERS 12 October 1964

SELF-TRAPPING OF OPTICAL BEAMS*

R. Y. Chiao, E. Garmire, and C. H. Townes
Massachusetts Institute of Technology, Cambridge, Massachusetts
(Received 1 September 1964)

$R = f(I, n_{eff})$

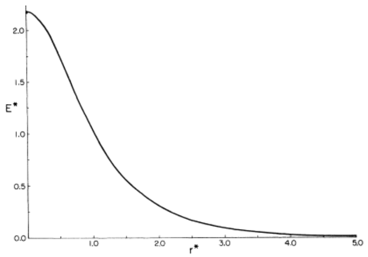

FIG. 1. Calculated radial distribution of the electric field in a self-trapped electromagnetic wave.

Kerr effects

Molecular orientation, electrostriction, electronic polarizability

SOVIET PHYSICS JETP VOLUME 23, NUMBER 6 DECEMBER 1966

SELF-FOCUSING AND SELF-TRAPPING OF INTENSE LIGHT BEAMS IN A NONLINEAR MEDIUM

S. A. AKHMANOV, A. P. SUKHORUKOV, and R. V. KHOKHLOV
Moscow State University
Submitted to JETP editor December 14, 1965
J. Exptl. Theoret. Phys. (U.S.S.R.) 50, 1537–1549 (June, 1966)

beams become self-trapped in a medium with $n_2 > 0$ and $n_4 < 0$. The diameter of such a self-trapped beam oscillates;

Wakefield acceleration of electrons

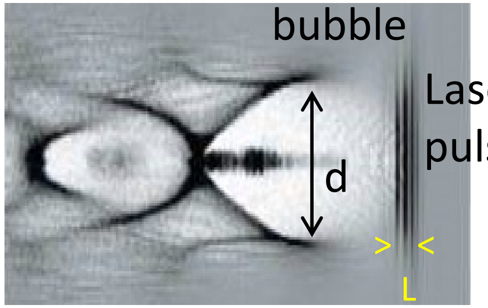

$0.004n_c$

Tajima T. and Dawson J. M. 1979 Phys. Rev. Lett. **43** 267

3D plasma wave

Pukhov A. and Meyer-ter-Vehn J., 2002 Appl. Phys. B: Lasers Opt. **74** 355

"bubble" regime

$$L < \lambda_p \quad L < d$$

Quasi-monoenergetic electrons, pC charge

Up to 3 GeV (gas jet) and 4.2 GeV (capillary)

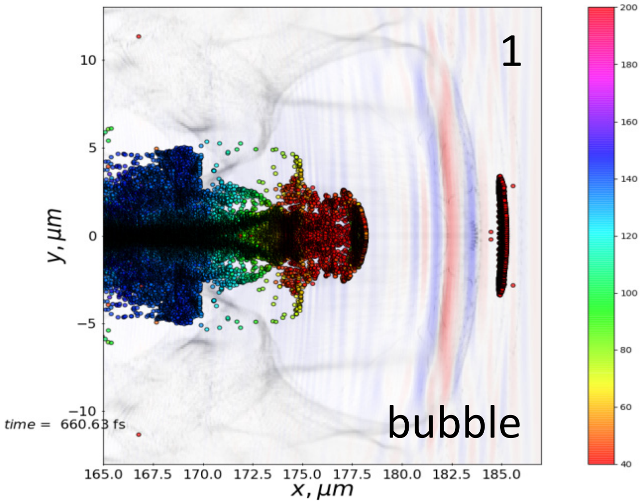

$\cancel{L < \lambda_p \quad L < d}$

$L > \lambda_p$, $L > d$

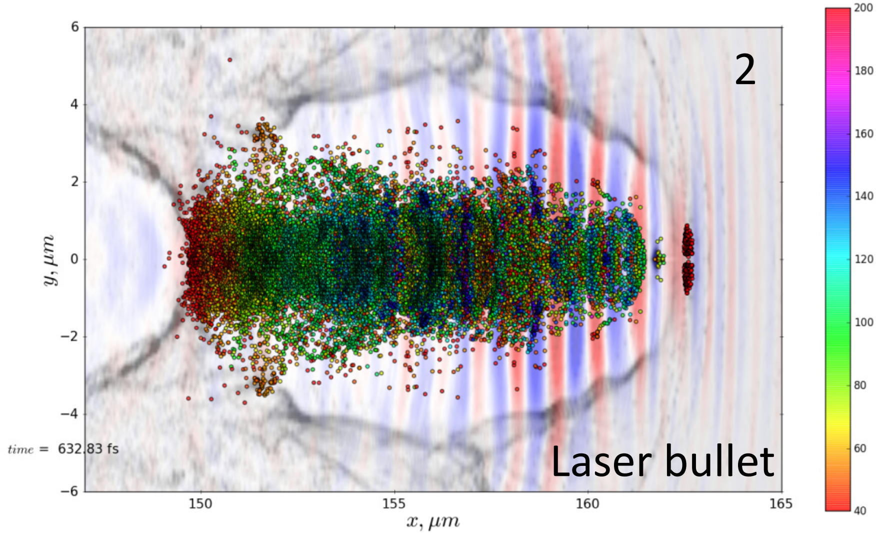

$a_0 = 10$, $R = 10\lambda$, $\tau = 13$fs, $n_e=0.04n_c$

$E_1/E_2 \approx 2$

$a_0 = 24$, $R = 2\lambda$, $\tau = 30$fs, $n_e=0.1n_c$

Laser light self-trapping regime

n_e=0.1n_c

Propagation over ~ 10 Rayleigh lengths

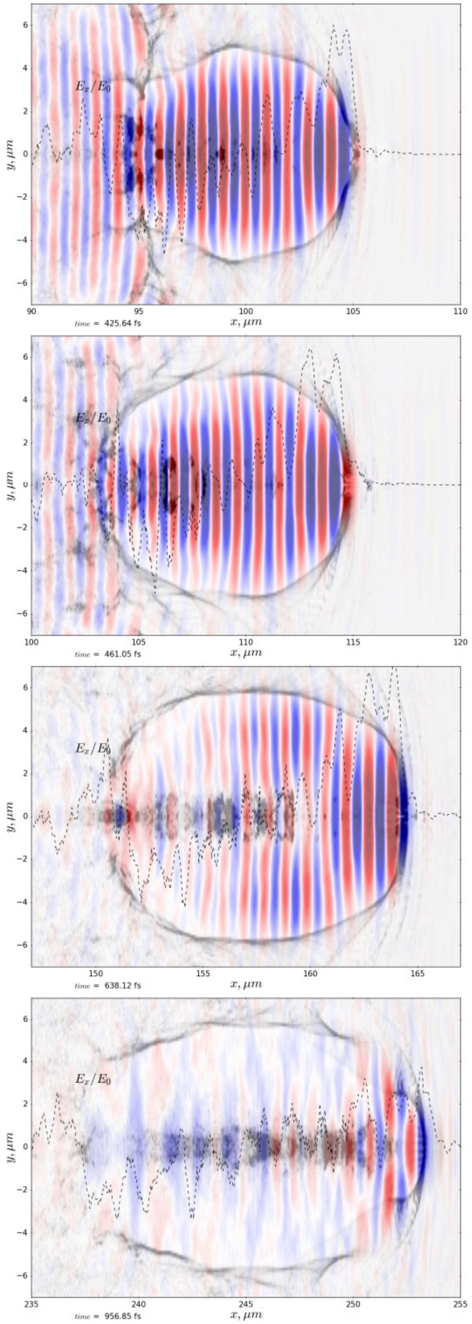

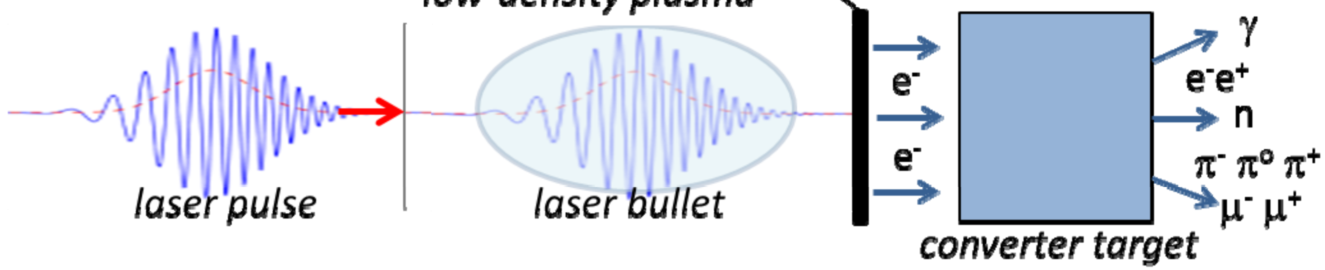

$$R \cong \frac{c}{\omega_p}\alpha\sqrt{a_0}$$

a_0= 0.85λ[μm]$\sqrt{I[W/cm^2]}\times 10^{-9}$ α - numeric factor ~ (1-2)

a_0 = 24, R_L = 2λ, τ = 30fs, P = 100 TW

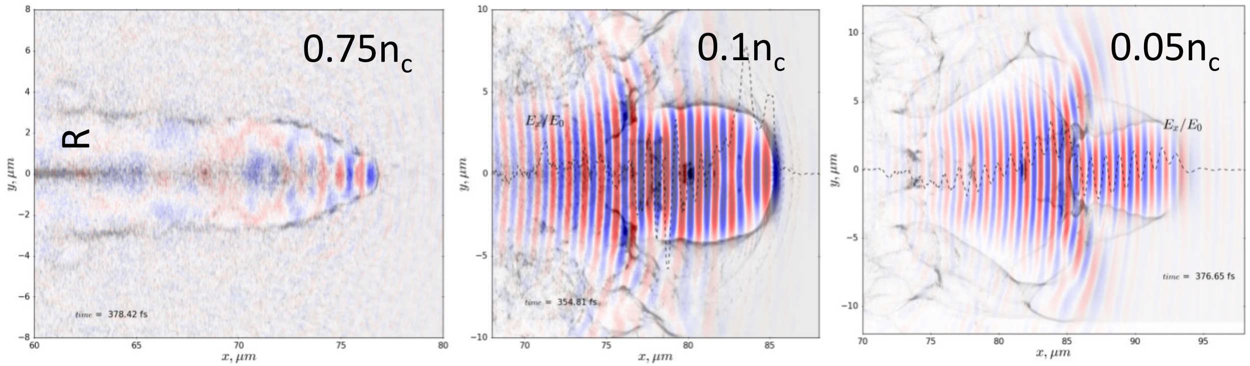

R (n, I) - matching

Matching condition ≡ relativistic (a>>1) self-trapping

Comparison of two self-trapping pulses with initial radius $R_L = 2\,\mu$m and amplitudes $a_0 = 24$ (left) and $a_0 = 72$ (right) propagating in plasmas with the corresponding electron densities $0.1 n_c$ and $0.3 n_c$

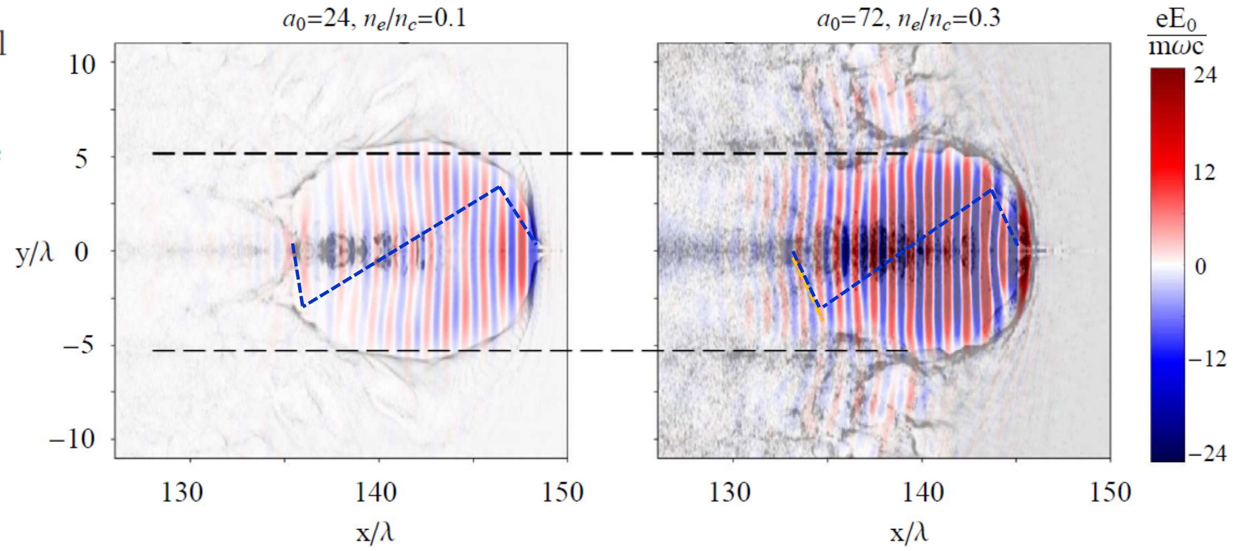

Laser pulse = soliton

$$\frac{R_1}{R_2} = \sqrt{\frac{a_1 n_2}{a_2 n_1}}$$

Comparison of two self-trapping pulses with the amplitude $a_0 = 24$ and initial radii $R_L = 2\,\mu$m (le and $R_L = 4\,\mu$m (right) propagating in plasmas wit the corresponding electron densities $0.1 n_c$ and $0.02 n_c$

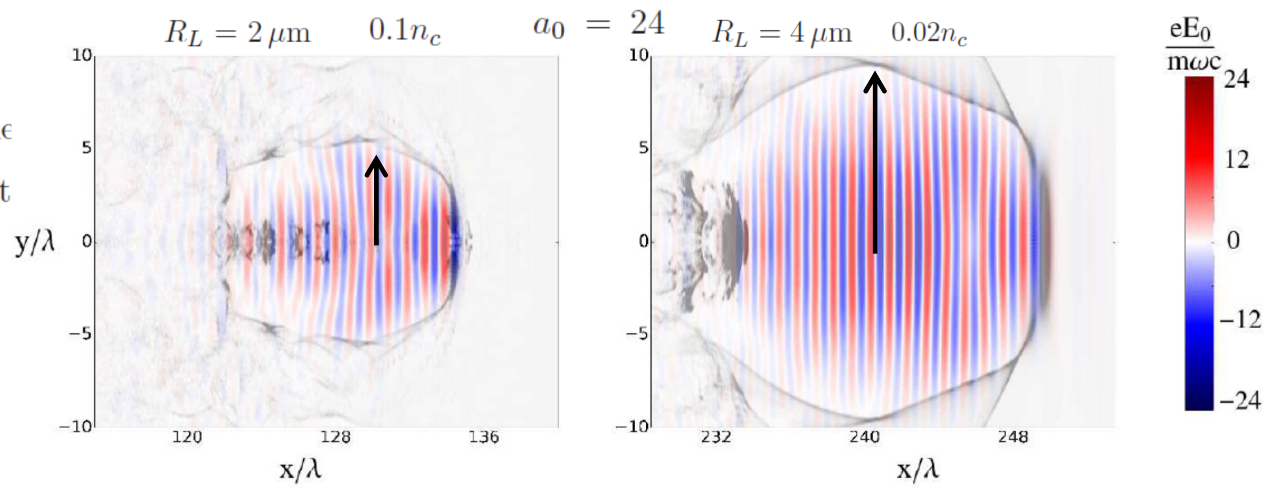

M.G.Lobok, A.V.Brantov, V.F.Kovalev, and V.Yu.Bychenkov
Plasma Phys. Contr. Fus. 61, 124004 (2019)

Physics of the matched cavern spot size condition

$$\boxed{R \cong \frac{c}{\omega_p}\alpha\sqrt{a_0}} \qquad R = \frac{c}{\omega}\sqrt{\frac{n_c}{n_e}}\left(\frac{16\alpha^4 P}{P_c}\right)^{1/6}$$

P – laser pulse power

1 Gordienko S and Pukhov A 2005 *Phys. Plasmas 12*, 043109 $\alpha \approx 1.12$

2 Lu M *et al* 2007 *Phys. Rev. STAB* **10**, 061301 $\alpha \approx 2$

3 Lobok M G Brantov A V Gozhev D A and Bychenkov V Yu 2018 *Plasma Phys. Control. Fusion* **60** 084010 $\alpha \approx 2$

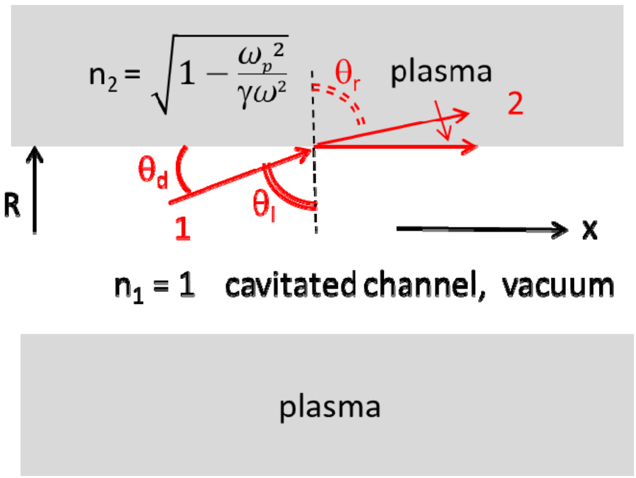

Snell's law

$$\theta_d \simeq \lambda/\pi R \qquad \theta_i = \pi/2 - \theta_d$$

$$n_1 \sin\theta_i = n_2 \sin\theta_r$$

condition of the total internal reflection, $\theta_r = \pi/2$

$$\theta_d^2 \simeq \left(\frac{2c}{\omega R}\right)^2 \simeq \frac{\omega_p^2}{\gamma\omega^2} \simeq \frac{\sqrt{2}\omega_p^2}{a_0\omega^2} \qquad \gamma = \sqrt{1 + a_0^2/2} \simeq a_0/\sqrt{2}$$

$$\boxed{R \cong \frac{c}{\omega_p} 2^{3/4}\sqrt{a_0}}$$

Laser beam self-trapping: plane geometry

NLSE + relativistic nonlinearity of electron mass

$$2ik\partial_z E + \partial_{xx}E + k^2\frac{\epsilon_{\rm nl}}{\epsilon_0}E = 0,\ E = A\exp\left(i\frac{\nu z}{2kd^2}\right),\ \gamma = \sqrt{1+|E/E_{\rm rel}|^2},\qquad \boldsymbol{E=E(x,z,\ t-z\sqrt{\varepsilon_0}/c)},$$

$$\epsilon_0 = 1 - \frac{4\pi e^2 n_{e0}}{(m_0\omega^2)},\ \epsilon_{\rm nl} = \epsilon_0\frac{k_p^2}{k^2}\left(1-\frac{1}{\gamma}\right),\ k_p^2 = \frac{4\pi e^2 n_{e0}}{m_0 c^2},\ k = \frac{\omega}{c}\sqrt{\epsilon_0},\ E_{\rm rel}^2 = \left(\frac{\omega c m_0}{e}\right)^2.$$

In dimensionless variables $z/2kd^2$, x/d, A/A_0, the solution depends upon two parameters:

$\rho = \omega_{\rm pe}d/c$ and $i_0 = (e/\omega m_0 c)^2 A_0^2 = I_0/I_r$, with $I_0 = (c/4\pi)A_0^2$, $I_r = \omega^2 m_0^2 c^3/(4\pi e^2)$.

Self-trapping solution for $\nu = \rho^2(1+(2/i_0)(1-p_0))$

$$\sqrt{\frac{2}{(p_0+1)}}\rho x = -\pi + 2\arctan\sqrt{\frac{p+1}{p_0-p}} - \sqrt{\frac{2}{p_0-1}}\ln\frac{2\sqrt{p_0-p}+\sqrt{2(p_0-1)(p+1)}}{\sqrt{2(p_0+1)(p-1)}},$$

$$p_0 = \sqrt{1+i_0},\quad p = \sqrt{1+i_0A^2},$$

Limiting case $\quad i_0 \to 0: \quad A^2 = \cosh^{-2}\left(x\rho\sqrt{i_0}/2\right).$

$$\Delta x\omega_{pe} \sim \frac{m_e}{a_0} \to \frac{\Delta x}{\sqrt{m_e}} \sim \frac{m_e}{a_0} \to \Delta x \sim \frac{(m_e)^{3/2}}{a_0} \sim a_0^{1/2}$$

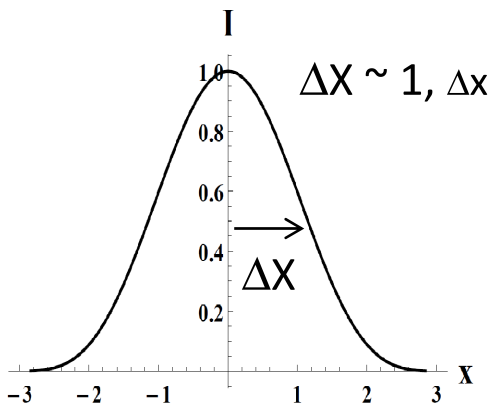

$\Delta X \sim 1,\ \Delta x \sim c a_0^{1/2}/\omega_{pe}$

$$x \equiv \sqrt{2/(p_0+1)}\rho x,\ \ I \equiv A^2.$$

Analytical theory of relativistic self-focusing

$$2ik\partial_z E + \triangle_\perp E + k^2(\epsilon_{nl}/\epsilon_0)E = 0\,, \; E(0,\mathbf{r}) = E_0(\mathbf{r})$$

$$\epsilon_{nl} = \epsilon_0 \frac{k_p^2}{k^2}\left(1 - \frac{n_e}{\gamma n_{e0}}\right) \qquad \gamma = \sqrt{1 + |E/E_{rel}|^2}$$

$$E_{rel}^2 = (\omega c m_0/e)^2$$

$$N_e = \frac{(1 + k_p^{-2}\triangle_\perp\gamma)}{(1 - \exp(-\alpha_0(1 + k_p^{-2}\triangle_\perp\gamma)))} \qquad n_e = n_{e0}N_e(\gamma)$$

relativistic electron mass + and ponderomotive charge-displacement

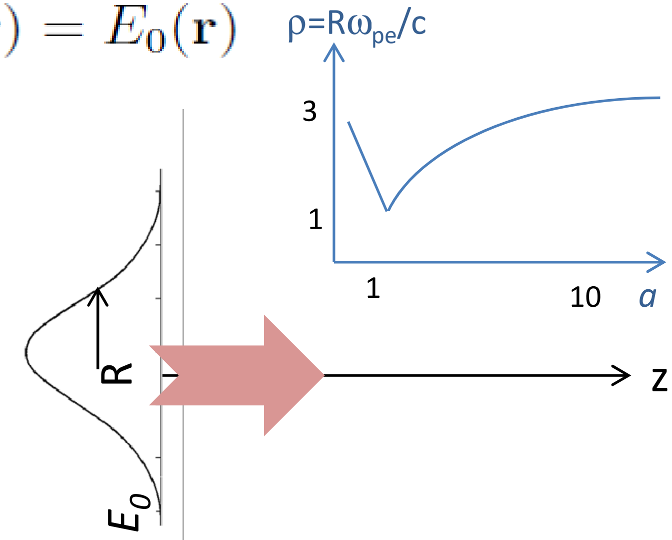

Gaussian radial intensity distribution at the plasma boundary

V.F.Kovalev & V.Yu.Bychenkov
Phys. Rev. E **99**, 043201 (2019)

- **Search for new regimes of relativistic self-focusing**

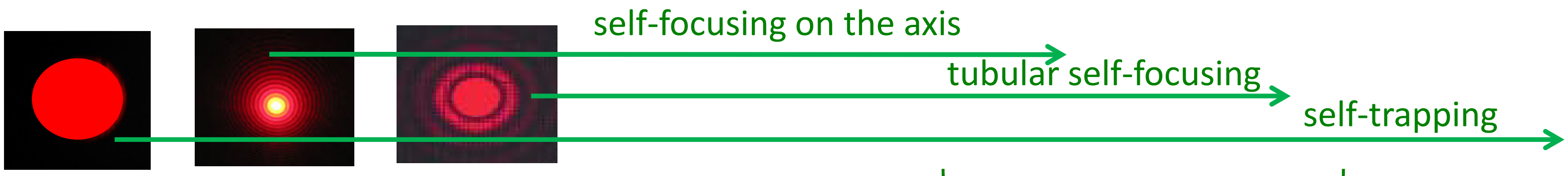

- **Finding of window parameters for different regimes of channeling**

three stationary self-focused waveguide propagation modes

Self-trapping: $R\omega_p/c = F(a_0)\,,\; a_0 \gg 1 \rightarrow R\omega_p/c \sim \sqrt{a_0}$ → balance of forces; → no filamentation

Electron acceleration. Stochastic injection.

Etching rate → optimum target thickness:
C.D.Decker *et al.*, Phys. Plasmas **3**, 2047 (1996)

$L_{dep}=L_{etch} \approx c\tau(n_c/4n_e)a_0$

High conversion to MeV electrons (E>30 MeV) 15 %!

$a_0 = 12 \div 72$

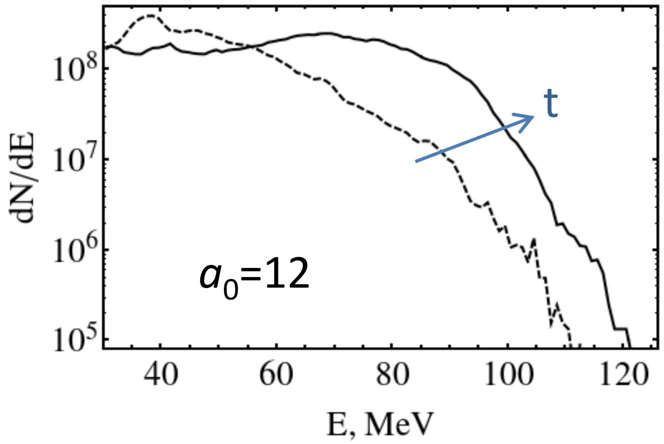

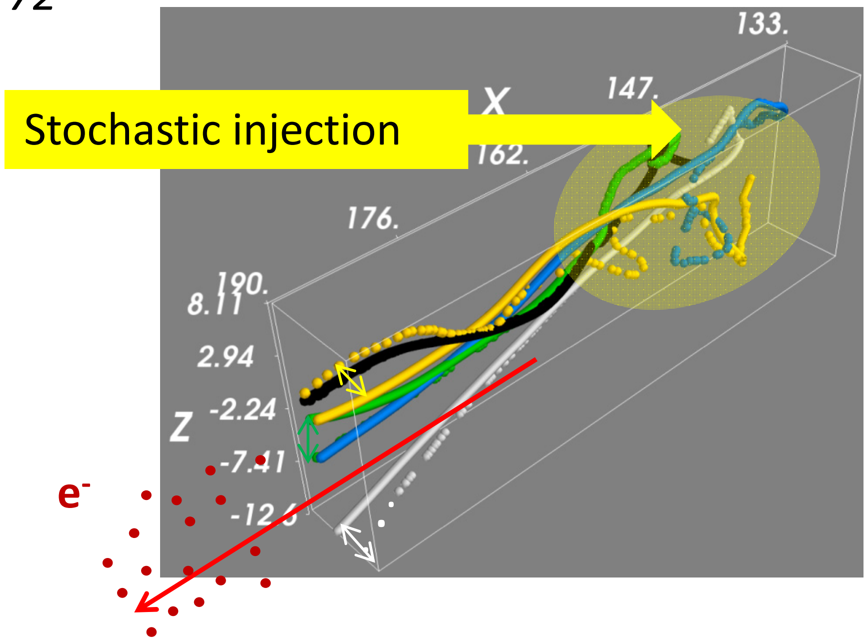

Generated electron beam

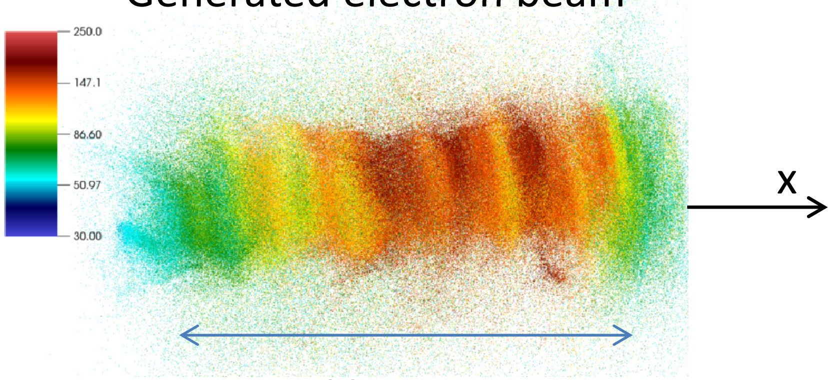

M.G.Lobok, A.V.Brantov, D.A.Gozhev, and V.Yu.Bychenkov
Plasma Phys. Contr. Fus. 60, 084010 (2018)

Intensity dependence

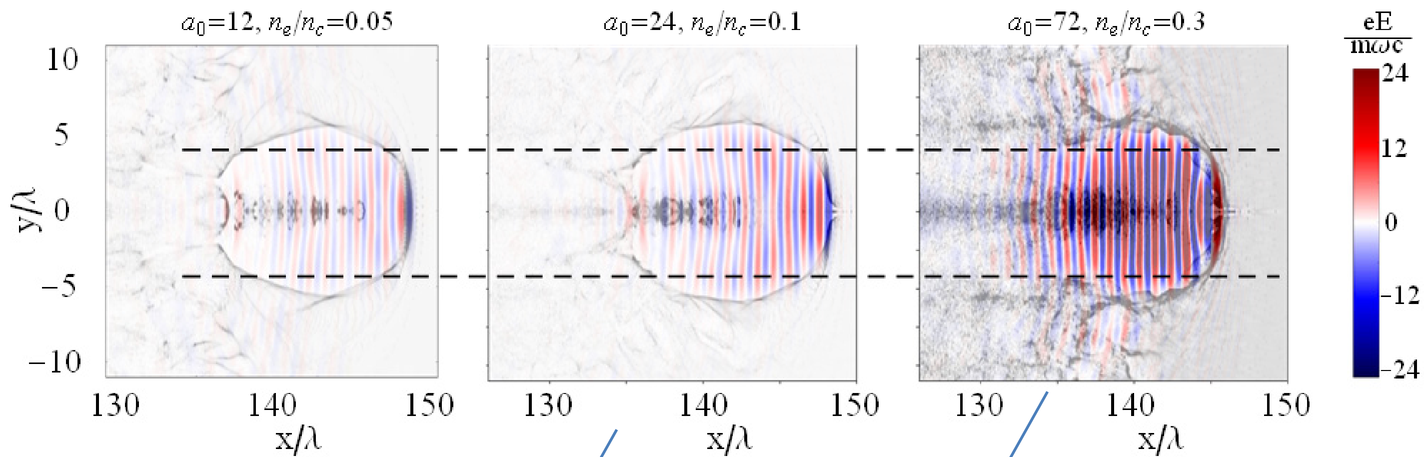

Very universal plateau-type spectra

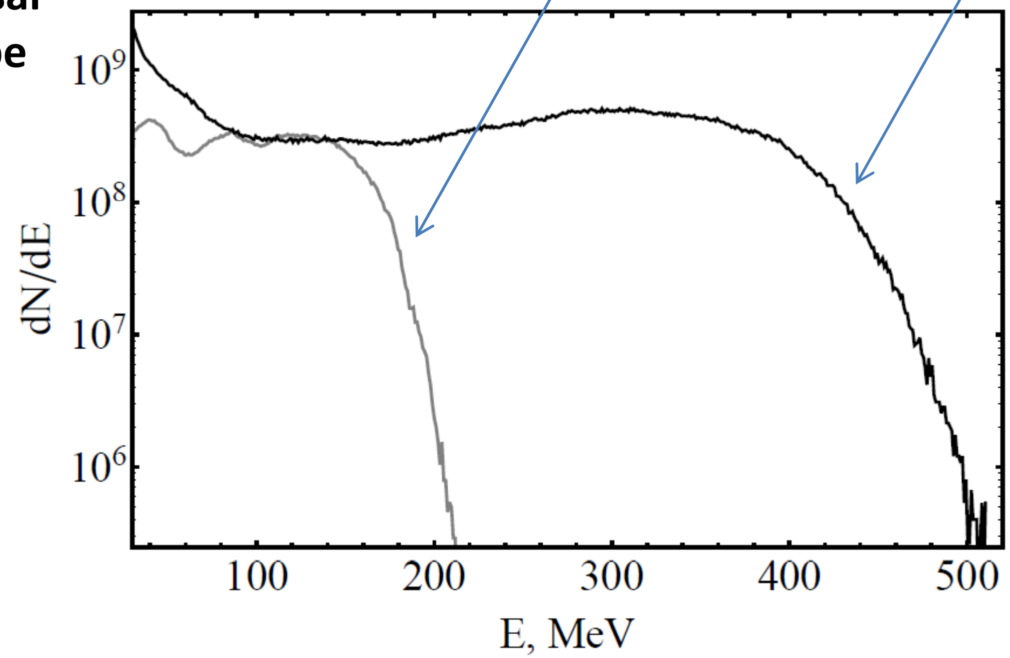

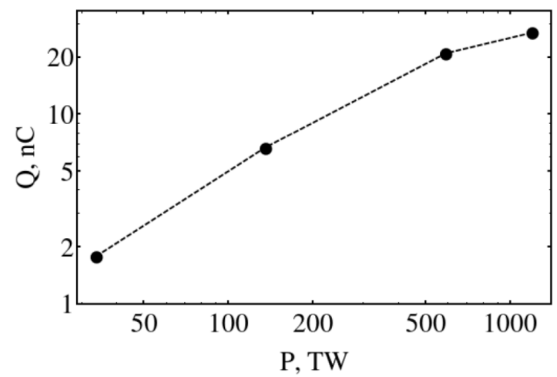

Dependence of the maximum total electron charge on the laser power for a 30 fs pulse

Electron spot

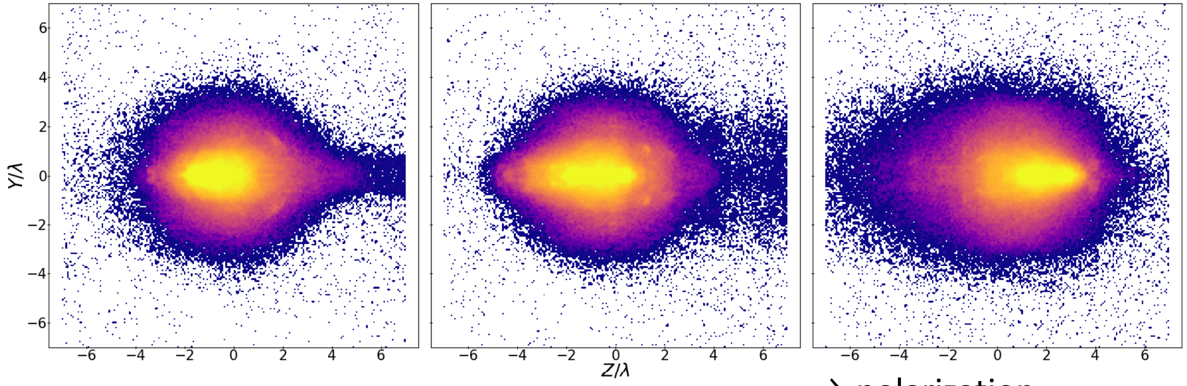

$$\Delta z \approx 0.16\lambda a_0$$

$$T \approx 0.25\lambda a_0^2/c$$

electron divergence is approximately 50 mrad, that corresponds to the emmitance of about 0.1 rad×μm

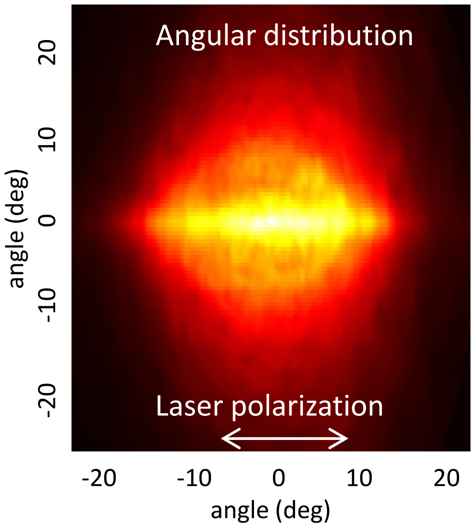

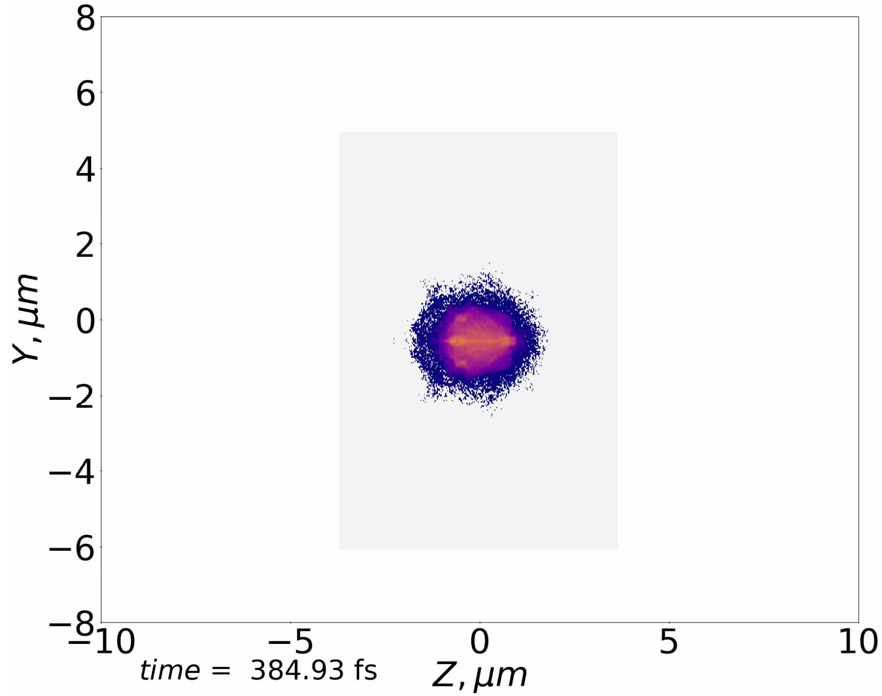

face pics

Hard x-ray betatron radiation

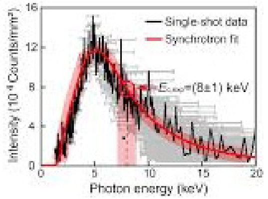

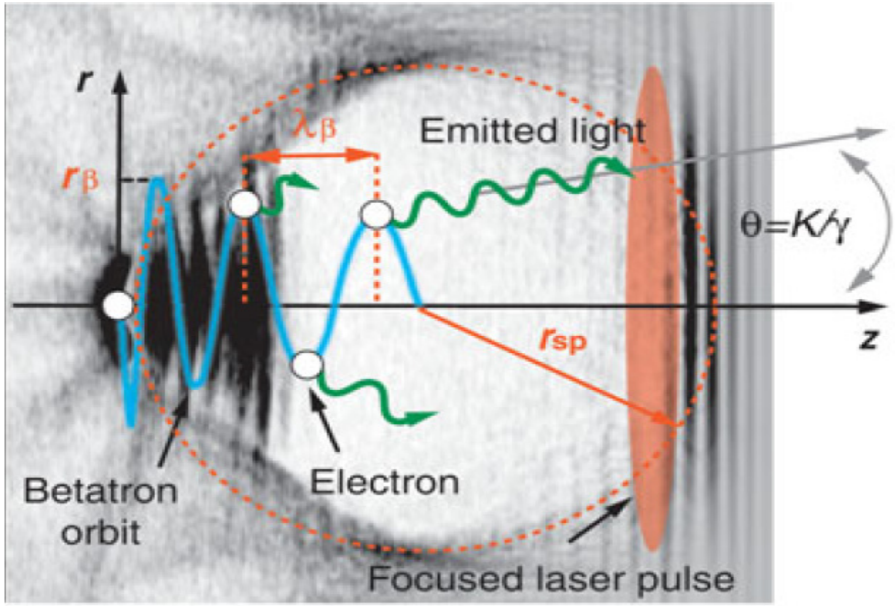

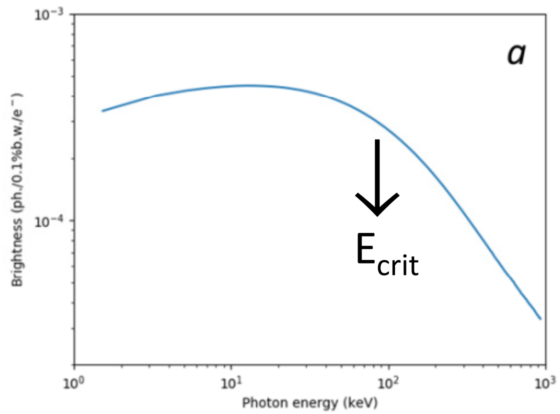

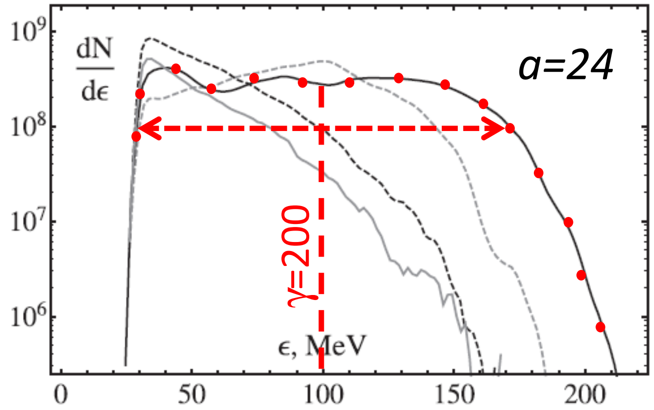

Energy spectra of high-energy (>30 MeV) electrons leaving optimum thickness targets of different densities $1n_c$ (gray curve), $0.75n_c$ (black dashed curve), $0.1n_c$ (black curve), and $0.05n_c$ (gray dashed curve).

$$E_{\text{crit}} = \hbar\omega_{\text{crit}} \simeq 5 \times 10^{-24}\gamma^2 (n_e/\text{cm}^{-3})(r_\beta/\mu\text{m})\text{keV}$$

γ = 200, $n_e = 20^{20}$ cm^{-3}, r_β= 5 μm

E_{crit} = 100 keV

Betatron emission I

Randomly chosen (1-1.5)$\times 10^4$ trajectories of high-energy electrons
+ Lienard-Wiechert vector potential approach

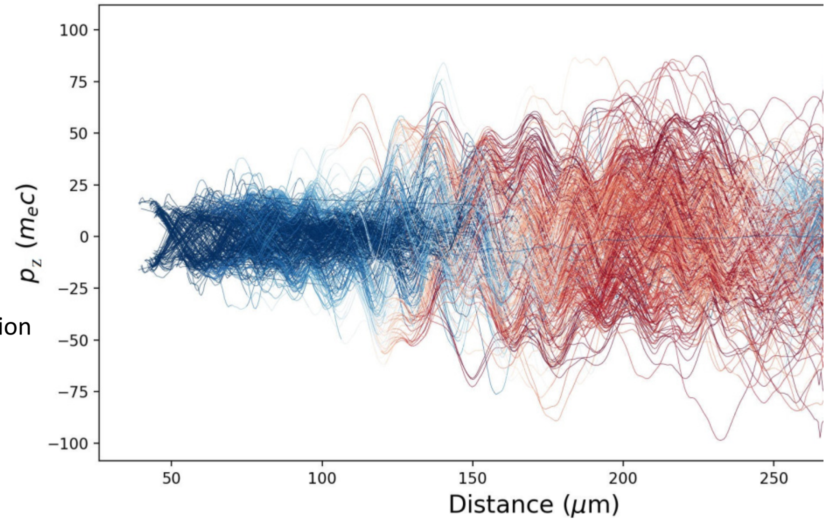

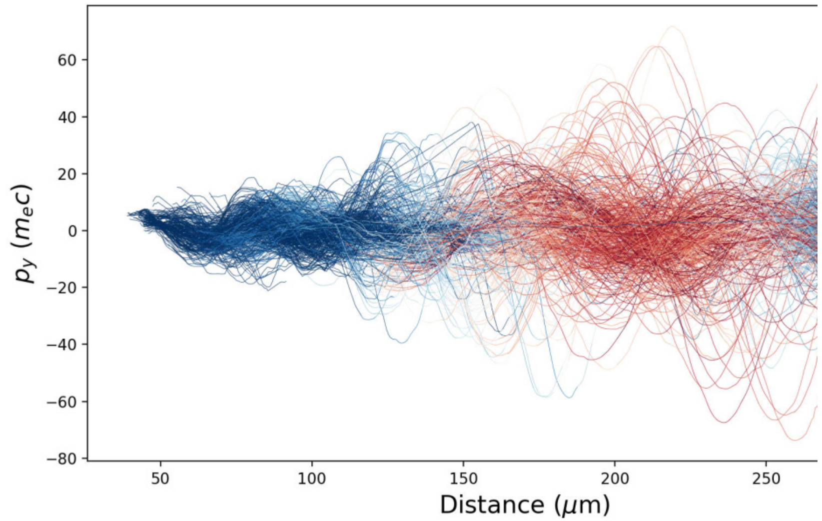

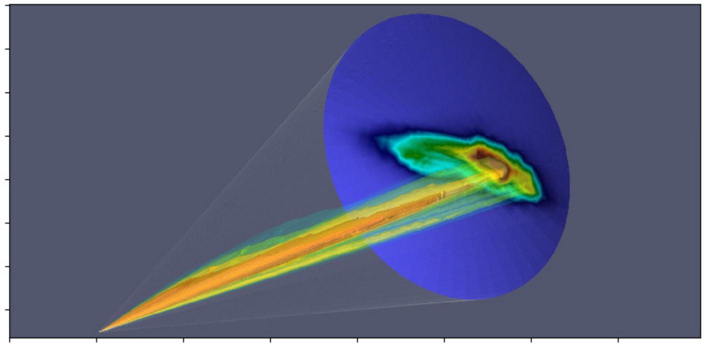

$$a_0 = 24 \Rightarrow \simeq 8\times 10^{20}\ \mathrm{W/cm^2}$$

130 TW

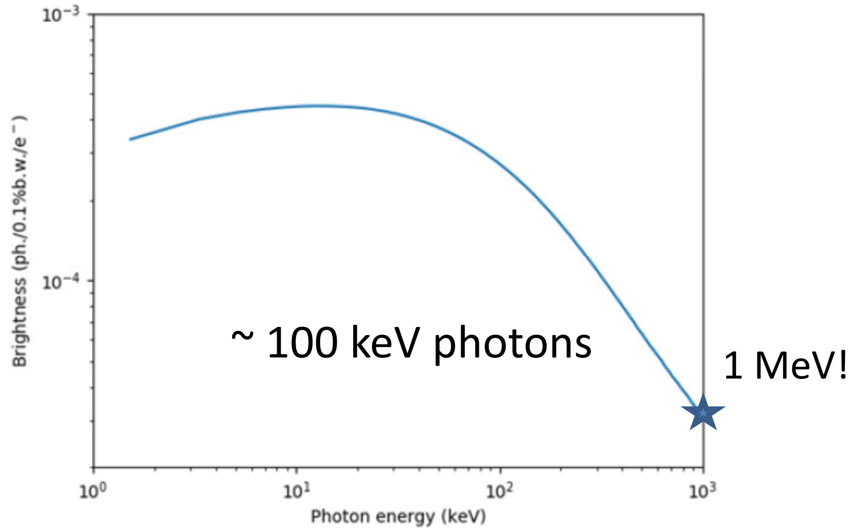

Betatron emission II

peak brightness, > 100keV
10^21 ph/0.1%b.w./mrad^2/mm^2/s

X-ray distribution

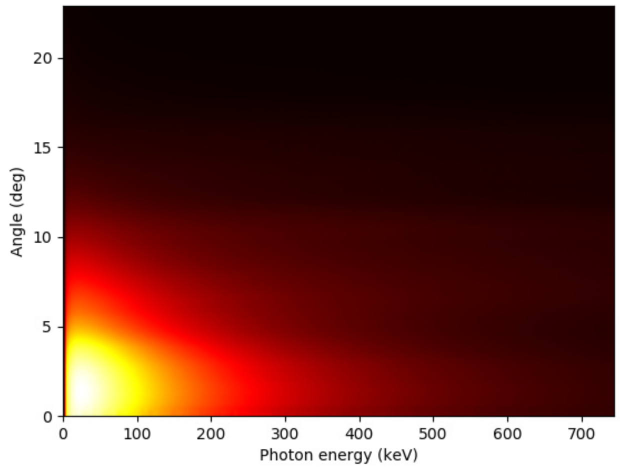

polarization degree, $P \simeq 1/3.$

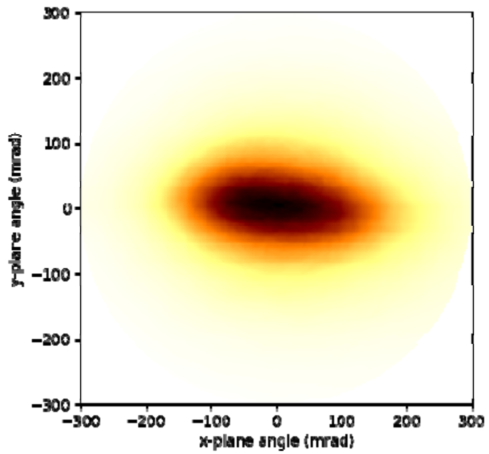

x-ray emission spot

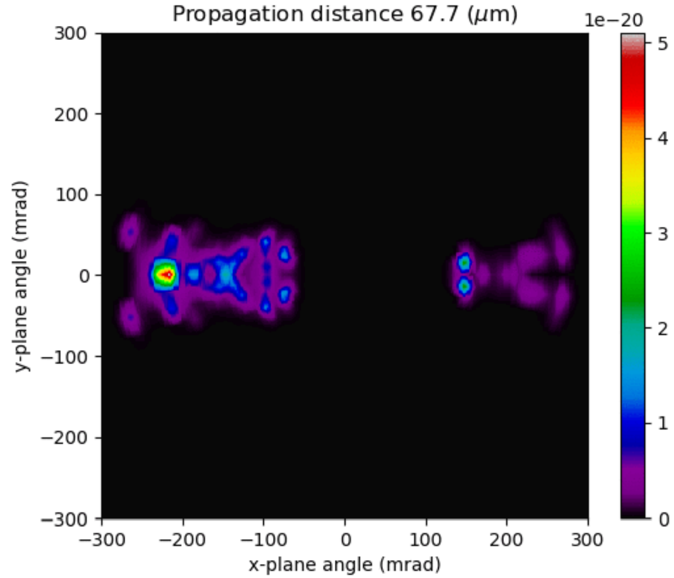

Spectral-angular distribution of the photons (from the electrons with energy > 30 MeV) in a far-eld zone.

5 ×10^{10} photons > 10 keV
Photon energy ~ 0.5 m J

To study magnetic materials
To study local electronic structure

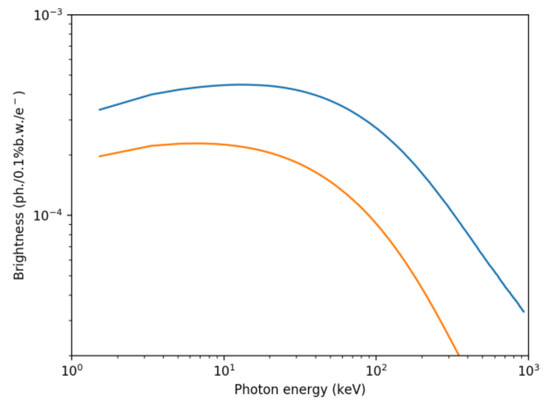

Strongly polarized x-rays

Electron conversion to gammas, e^-e^+, photonuclear products

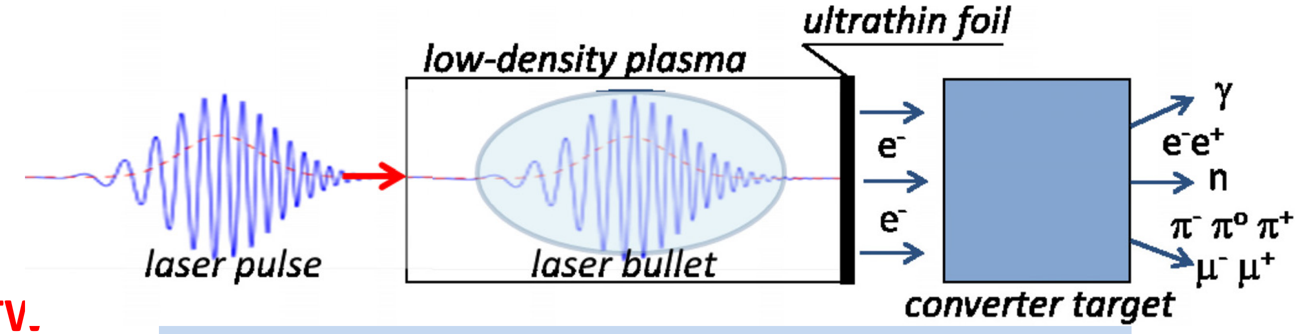

130 TW.

8×10^{20} W/cm^2, $\lambda=1\mu m$, 30fs, $d=4\mu m$, $n_e=0.1n_c$, Q=7nC

Converter

Pt194	Z = 78	N = 194	32.967 %
Pt195	Z = 78	N = 195	33.832 %
Pt196	Z = 78	N = 196	25.242 %
Pt198	Z = 78	N = 198	7.163 %

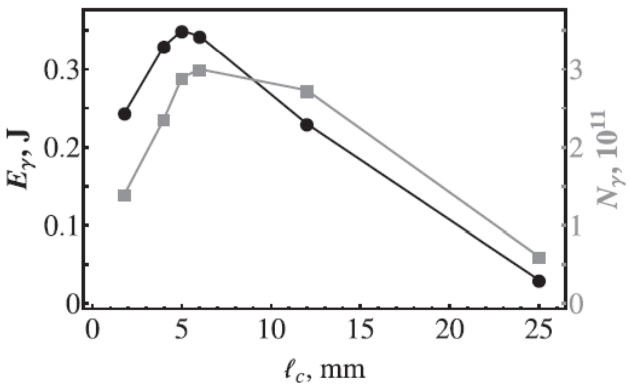

Total yield (left) and energy (right) of gamma rays vs the thickness l_c of the Pt converter target for the laser–plasma parameters $P = 130$ TW, $R_L = 2\lambda$, and $n_e = 0.1n_c$ corresponding to an electron bunch with $Q \simeq 7$ nC and an average energy of 100 MeV.

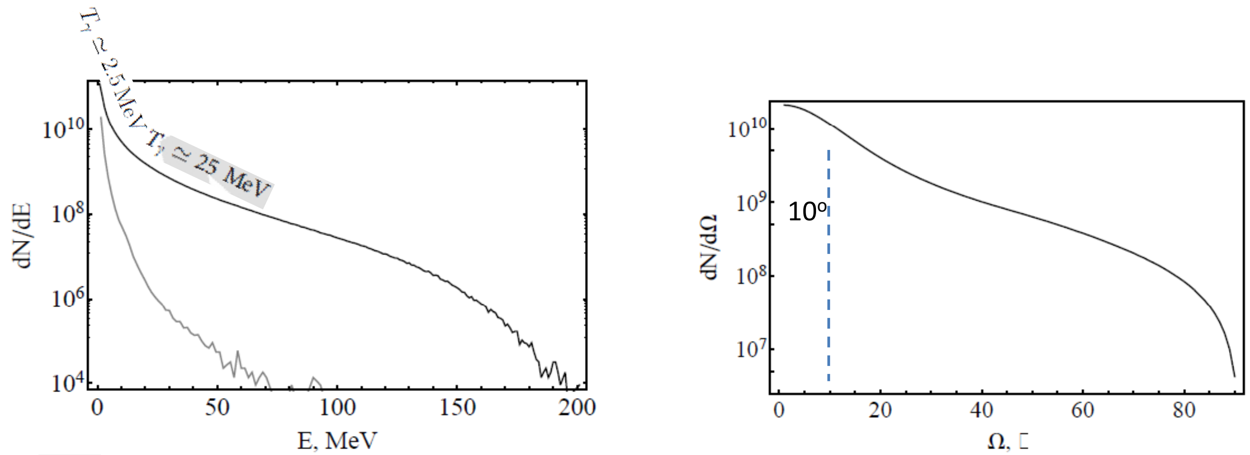

The energy spectra of gamma rays generated in the forward (black) and backward (gray) directions (left panel) and angular distribution of gamma-rays generated in the forward direction (right panel) from a 6 mm thick Pt target for the laser-plasma parameters $P = 130$ TW, $R_L = 2\lambda$, and $n_e = 0.1n_c$ corresponding to an electron bunch with $Q \simeq 7$ nC and an average energy of 100 MeV.

3×10^{11} photons, $\sim$0.35 J $\sim$8% laser-to-gamma conversion efficiency,

10 MeV gamma brightness $\sim10^{19}\ \mathrm{s^{-1}\ mrad^{-2}\ mm^{-2}\ (0.1\%\ BW)^{-1}}$

γ spot size and duration
60 μm, 300 fs

Single shot deep gamma-radiography (130 TW, 30 fs)

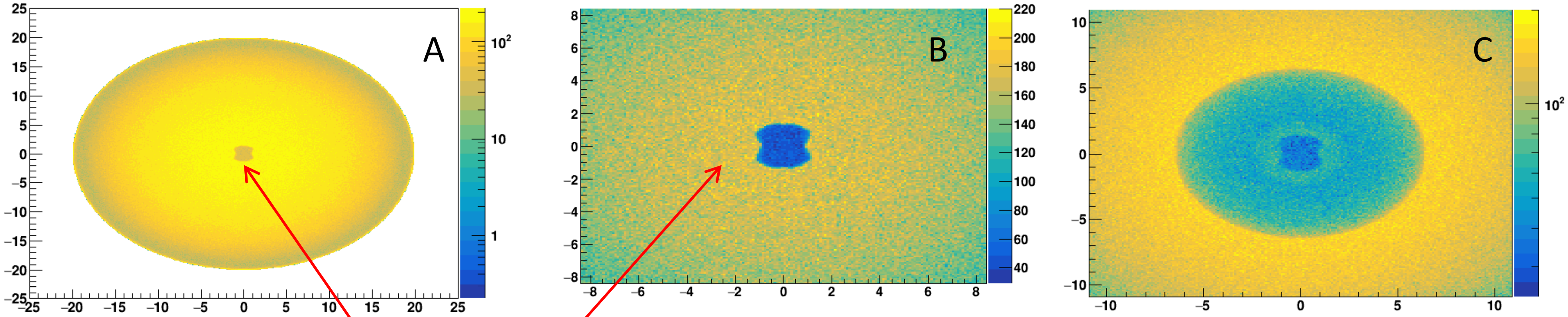

A crumpled platinum tube 5 meters from the converter, surrounded by a 3 cm iron shell (Fig. 2A, B). Fig. 2C: the platinum tube is additionally surrounded by a 10 cm aluminum shell. Detector dimensions in centimeters. Detector of the typical type used in PET imaging with a pixel size of (1-3) mm^2.

Mobile inspection system for special nuclear materials

Positron generation

Bether-Heitler

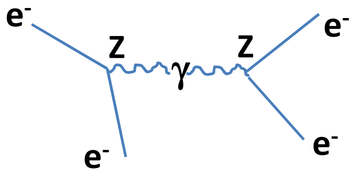

>

Trident

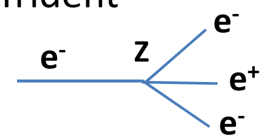

$n_{e+}=2\times10^{12}$ cm^{-3}

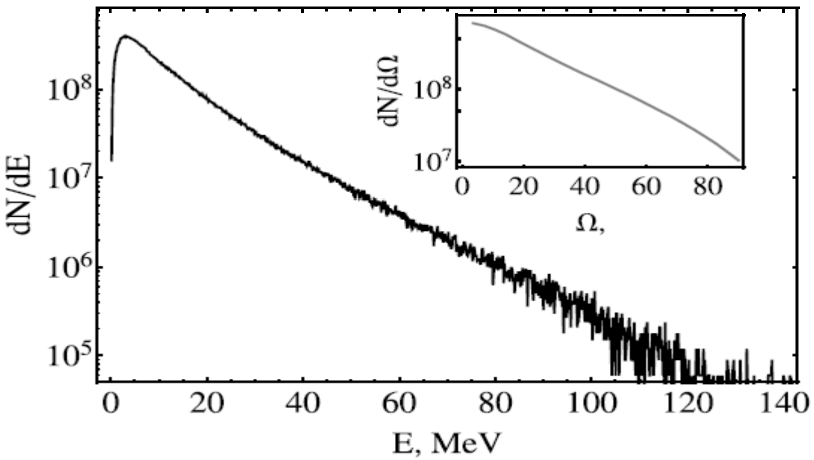

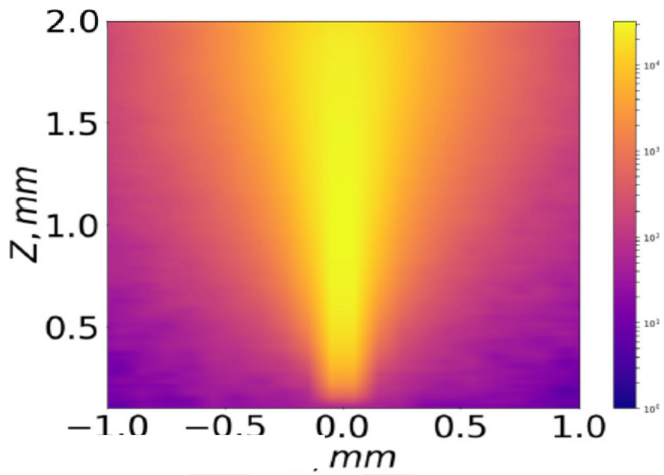

Energy spectrum of positrons generated from a 6 mm Pt target (left panel) and positron flux in a 1.8 mm Pt target (right panel) for the laser–plasma parameters $P = 130$ TW, $R_L = 2\lambda$, and $n_e = 0.1n_c$ corresponding to an electron bunch with $Q \simeq 7$ nC and an average energy of 100 MeV. The inset in the left panel shows the angular distribution of positrons generated from the 6 mm Pt target.

$N_{e+}= 9\times10^9$ 6 mm thick Pt target $N_e >> N_{e+}$

The positron jet angular spread increases from ~20^o for a 1.8mm Pt converter target to ~35^o for a 6mm target and ~40^o for a 12mm target.

Electron conversion to neutron emission

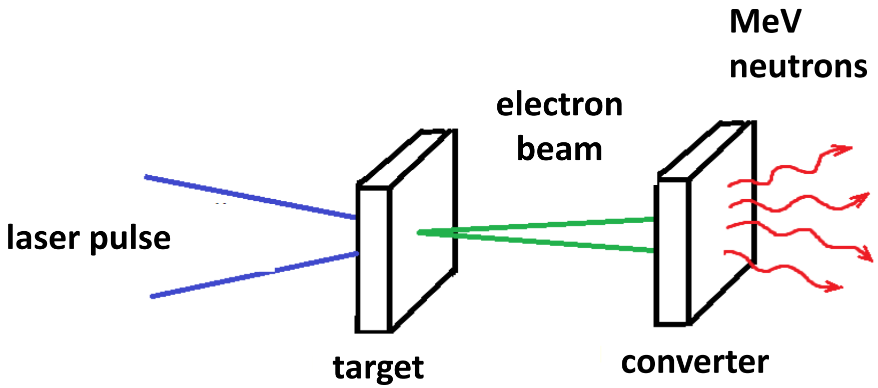

$8\times10^{20}W/cm^2$, $\lambda=1\mu m$, 30fs,
$d=4\mu m$, $n_e=0.1n_c$, Q=7nC

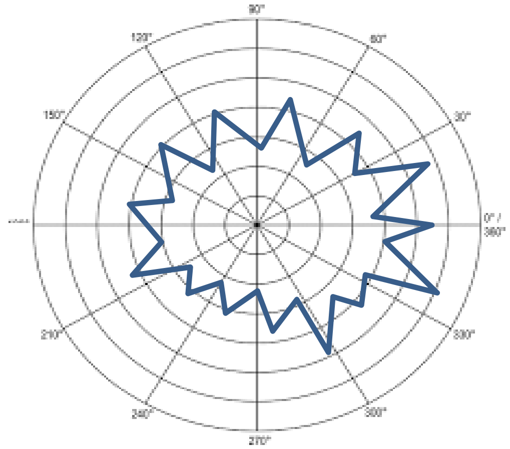

6.5×10^{-3} neutrons/electron

nearly isotropic neutron distribution

2×10^8 n°

dominance

$\underbrace{(\gamma,n), (\gamma,2n)}$, (γ,np), $(\gamma,3n)$, ...

highrep laser is required (kHz)

$K_n \sim 10^{-5}$

giant dipole resonance (GDR), 10 – 20 MeV

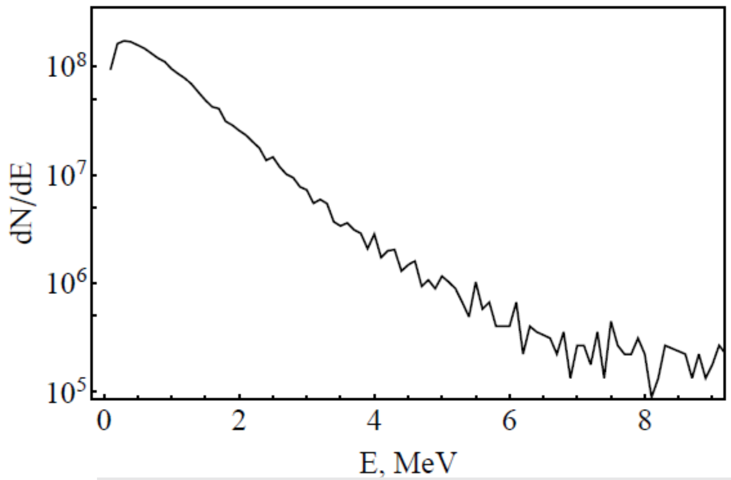

Energy spectrum of neutrons generated from a 12mm thick Pt target outside the target the forward and backward directions (at a 108° angle in both cases)

In general, photonuclear cross-section is smaller than typical nuclear cross sections due to the electromagnetic nature of interaction. However, at the resonance energy it is comparable on the order of magnitude with the geometrical nuclear cross section that well compensate a weakness of electromagnetic interaction.

PET isotope production (^{64}Cu)

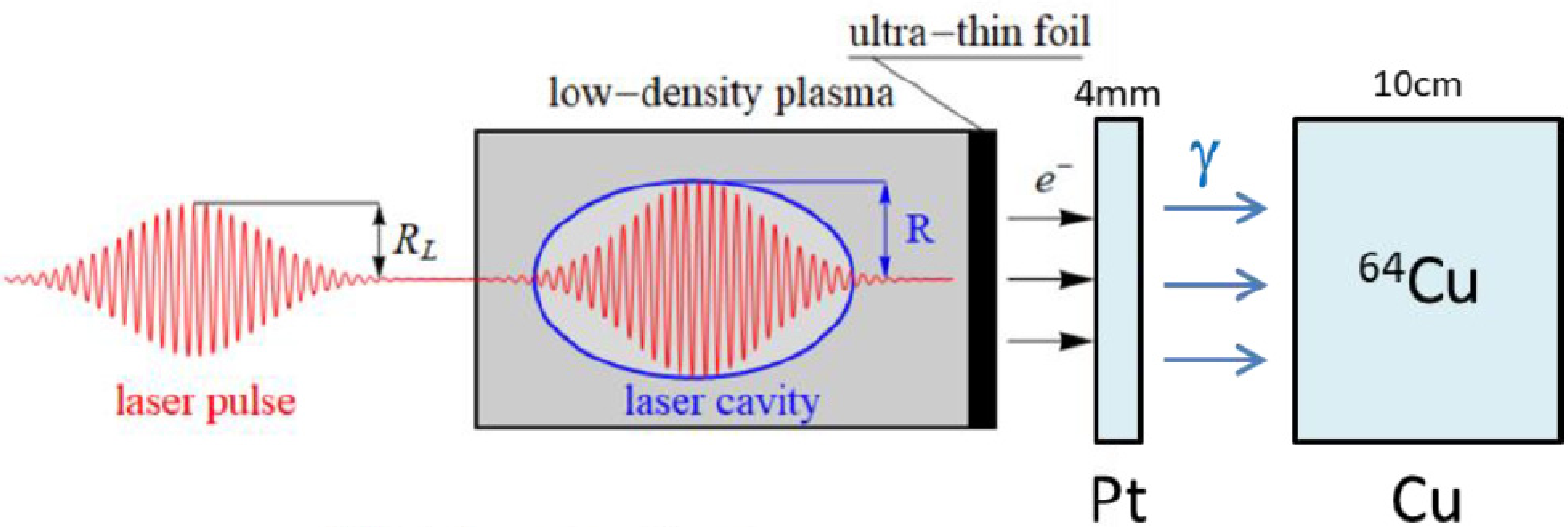

Numerical simulation scheme for isotope ^{64}Cu production for PET. Simulation parameters: P=130 TW, focal spot size = 6μm, pulse duration = 30 fs, plasma electron density = $0.1n_c$. **The yield of the isotope ^{64}Cu is 3×10^8**, that is unattainable for the reaction ^{64}Ni + p from a perfectly optimized scheme with an ultrathin solid dense foil (A.V.Brantov et al., Phys. Rev. AB 18, 021301 (2015)).

Photoproduction of mesons

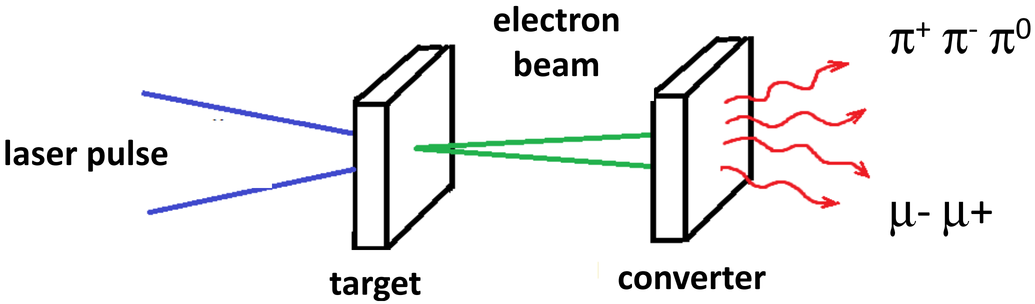

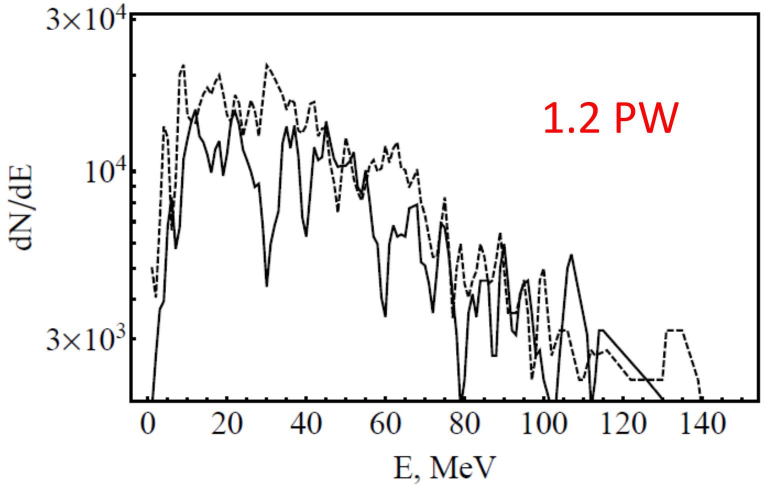

Spectra of photonuclear generated π^+ (solid line) and π^- (dashed line) pions

130 TW

$\pi^+ \approx \pi^0$ => 160, π^- => 210

Σ = 530

Cf. W. Schumaker et al., *New J. Phys.* **20**, 073008, 2018

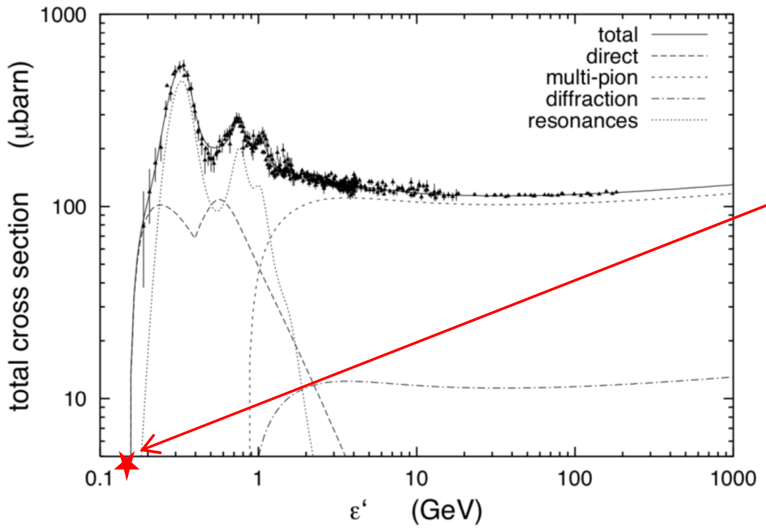

1.2 PW

$\pi^+ \approx \pi^0$ => 7×10^5, π^- => 1×10^6

unstable

$\Sigma = 2.4\times10^6$

μ^- μ^+ pairs were detected only from several PW pulse

Laser-triggered extreme THz fields and waves

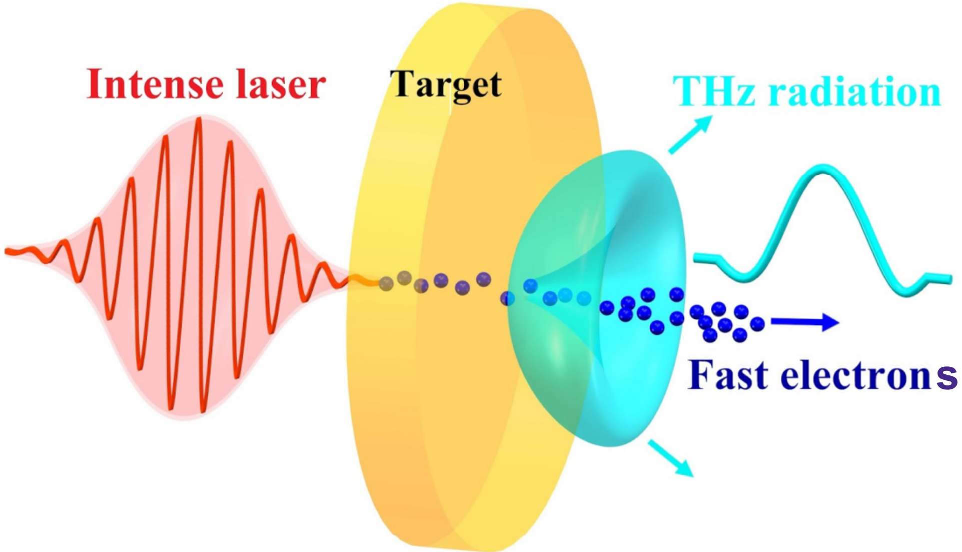

Volume THz radiation

Surface THz fields and waves

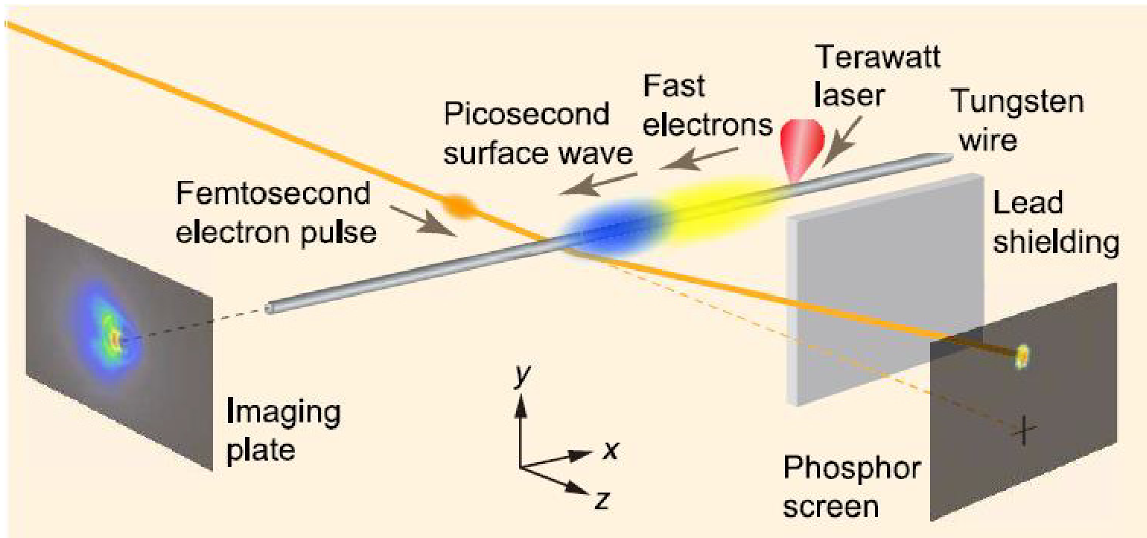

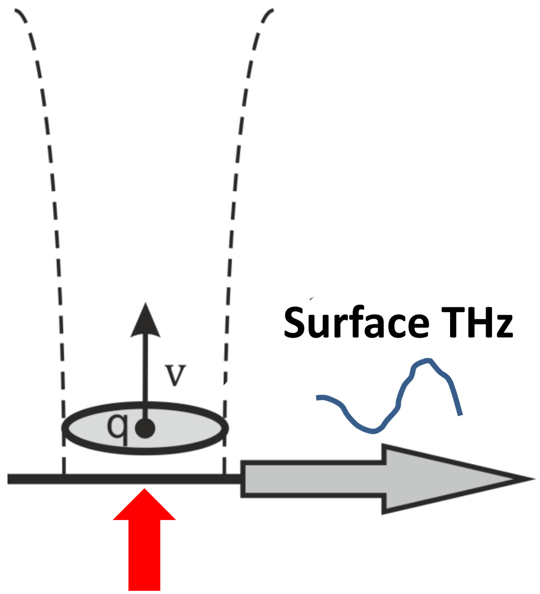

Mysterious waves. π - wave.

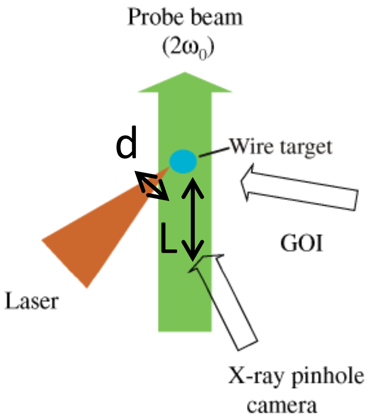

F. N. Beg et al.,
PRL 92, 095001 (2004)

VULCAN up to 5×10^{19} W/cm^2

L - several hundred microns
d $\sim$15 μm

induced MA-current along a wire !

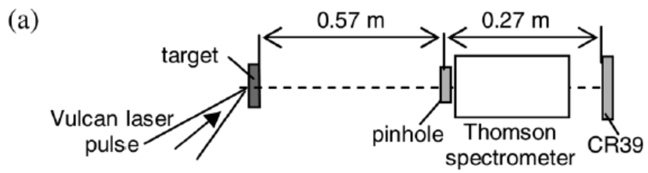

Ion acceleration

P. McKenna et al.,
PRL 98, 145001 (2007)

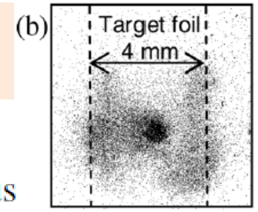

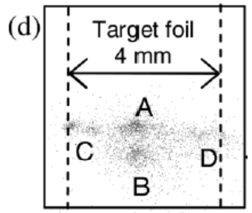

measurement of large electric fields ($\sim$0.1 TV/m) millimeters from the laser focus

K. Quinn et al., Phys. Rev. Lett. 102 194801 (2009)

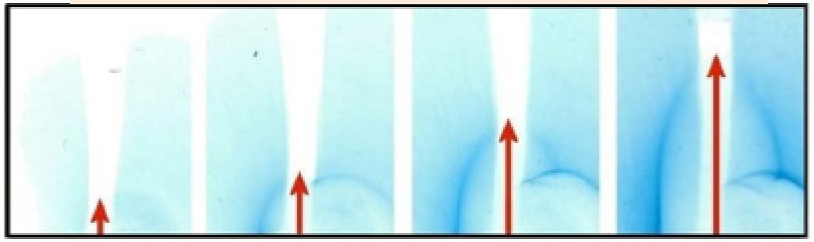

S. Kar et al., Nat. Commun. 7, 10792 (2016)

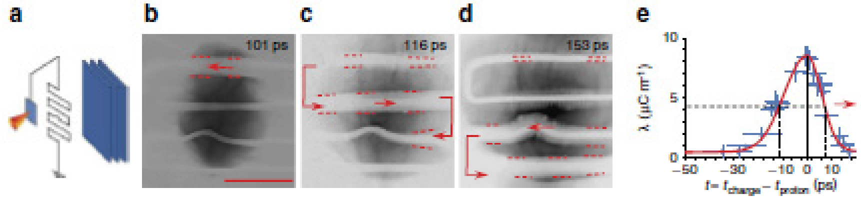

Tokita, S. et al. , PRL 106, 255001 (2011);
Sci. Rep. 5, 8268 (2015).

H. Nakajima et al.,
PRL 110, 155001 (2013)

R. Pompili et al.,
Sci. Rep. 8, 3243 (2018)

Relativistic electron beam guiding along a thin wire

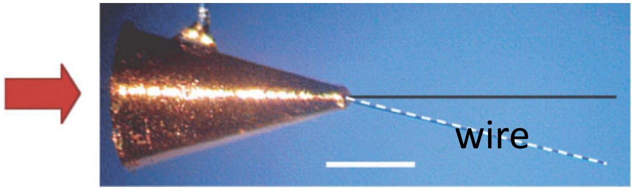

R. Kodama et al.,
Nature 432, 7020 (2004)
M. Borghesi et al.,
CLF Ann. Rep. 2006, p.13, Vulcan

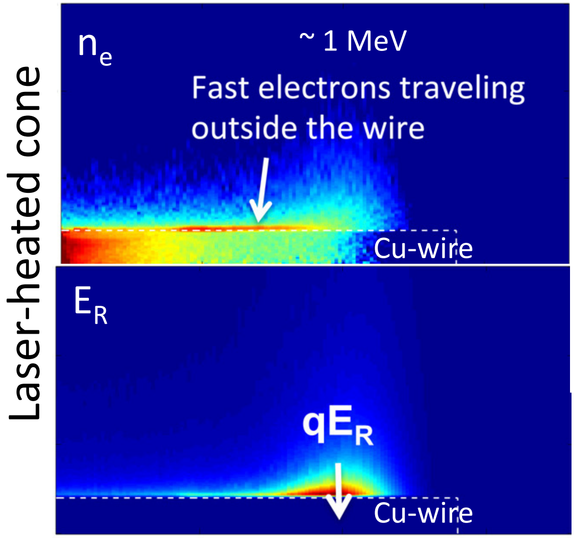

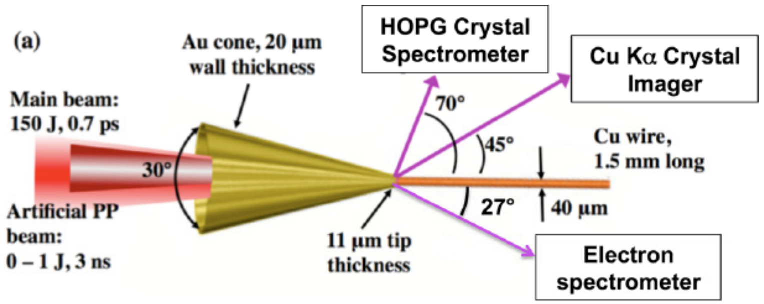

TITAN cone-wire experimental setup (LLNL, 2012)

S. Tokita et al.,
Sci. Rep. 5, 8268 (2015)

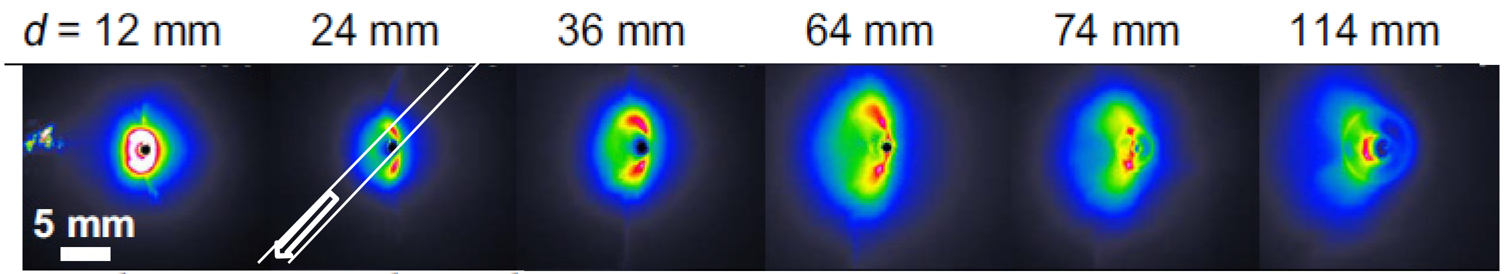

Fast electron images detected

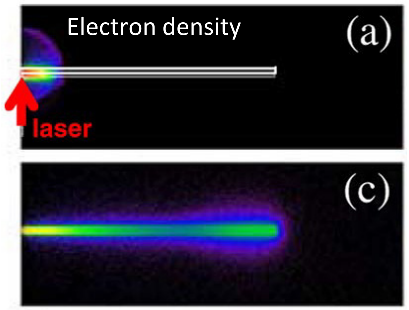

P. McKenna et al.,
PRL 98, 145001 (2007)

A.V.Brantov et al.,
EPJ Web Conf.
195, 03002 (2018)

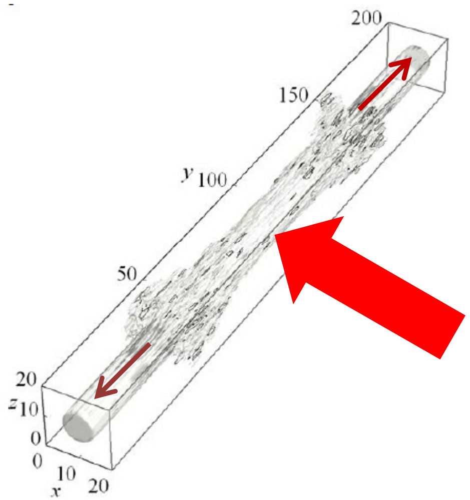

Theory of ultrafast target charging

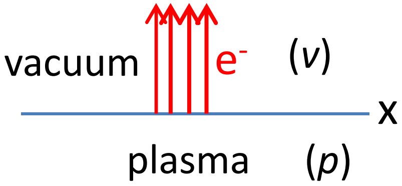

The full set of Maxwell equations with external current, **j** = en$_e$**v**

$$\frac{\partial^2 E_x^{p,v}}{\partial x^2} - k_{p,v}^2 E_x^{p,v} = \frac{4\pi e}{\epsilon}\frac{\partial \epsilon n^e_{\omega,k}}{\partial x} - \frac{4\pi e i\omega v}{c^2} n^e_{\omega,k} \qquad n_e = n^e(x - vt, \mathbf{r}_\perp)$$

$$\mathbf{k} \perp \mathbf{x},\ \mathbf{v} = (v,0,0),\ k_v = \sqrt{\mathbf{k}^2 - \omega^2/c^2},\ k_p = \sqrt{\mathbf{k}^2 - \epsilon\omega^2/c^2} \qquad n^e_{\omega,k} = n e^{i\omega x/v}/v$$

$$E_x^v = -\frac{4\pi e n k v}{v^2 k_v^2 + \omega^2}\left(\frac{i\omega}{kv}\left(1 - \frac{v^2}{c^2}\right) e^{i\frac{\omega x}{v}} + \right.$$
$$\left. + \frac{k(\epsilon - 1)(v k_p + i\omega(1 - v^2/c^2))}{(k_p + \epsilon k_v)(v k_p + i\omega)} e^{-k_v x}\right)$$

$$E_x^p = -\frac{4\pi e n k v}{\epsilon(v^2 k_p^2 + \omega^2)}\left(\frac{i\omega}{kv}\left(1 - \epsilon\frac{v^2}{c^2}\right) e^{i\frac{\omega x}{v}} + \right.$$
$$\left. + \frac{k(\epsilon - 1)(v k_v - i\omega(1 - \epsilon v^2/c^2))}{(k_p + \epsilon k_v)(v k_v - i\omega)} e^{k_p x}\right)$$

High-conductivity, $|\epsilon| \to \infty \quad E_x^p = 0$

The pole: $k_p + \epsilon k_v = 0, \qquad k_0 \simeq \pm\omega/c(1 - 1/(2\epsilon))$

$$\boxed{E_x^{sv} = -\int \frac{d\omega\, 2ienv\omega}{c^2\sqrt{-\epsilon}} e^{-i\omega(t \pm \frac{z}{c})} e^{-i\frac{\omega}{2\epsilon c}|z|} e^{-\frac{\omega x}{c\sqrt{-\epsilon}}}}$$

2D geometry, (x,z), filiform (along y) point charge

$$E^v_{x0} = \begin{cases} -\dfrac{4\lambda}{\sqrt{c^2t^2 - z^2}} \dfrac{cvt^2\gamma^2}{z^2 + v^2t^2\gamma^2}, & z^2 < c^2t^2, \\ 0, & z^2 > c^2t^2. \end{cases}$$

λ is the linear charge density

Polarization field

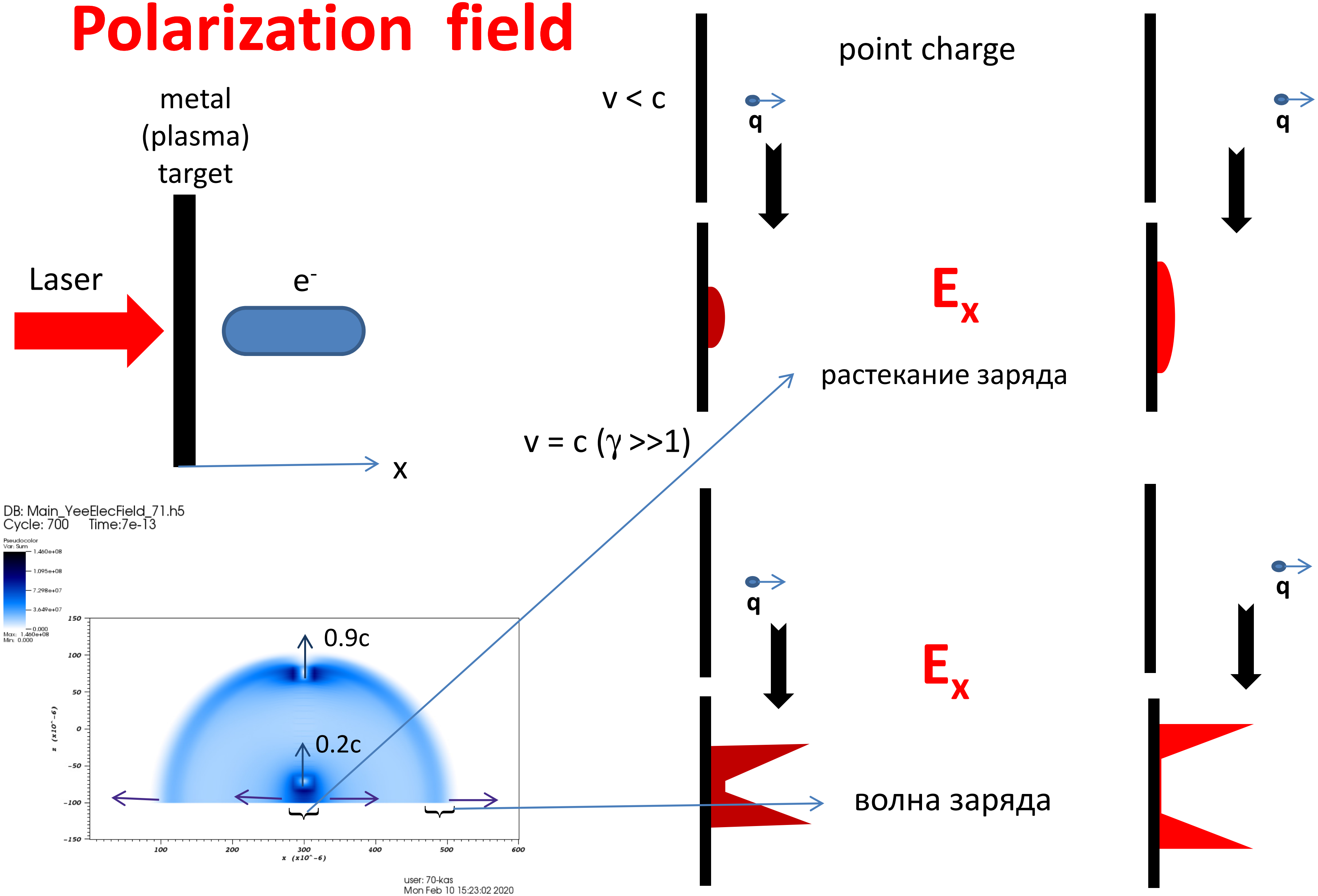

Ultrafast target charging due to polarization triggered by laser-accelerated electron bunches

The same physics holds for a finite-sized electron charge and is described analytically for |ε|>>1 and γ>>1 or γ<<1.

$$E_x^v = -\frac{4\pi ene^{-k_v x}}{ck_v}\,, E_x^p = \frac{4\pi en}{\epsilon}\left[\frac{e^{i\frac{\omega x}{c}} - e^{k_p x}}{i\omega} - \frac{e^{k_p x}}{ck_v}\right]$$

$$B_y^v = -\frac{4\pi en}{ck}\left(\frac{\omega}{ck_v}e^{-k_v x} - ie^{i\frac{\omega x}{c}}\right)\,,$$

$$B_y^p = -\frac{4\pi en}{ck}\left(\frac{\omega}{ck_v}e^{k_p x} - ie^{k_p x}\right)\,,$$

$$E_z^v = \frac{4\pi ien}{ck}\left(e^{-k_v x}\left[1 + \frac{\omega}{ck_p}\left(\frac{\omega}{ck_v} - i\right)\right] - e^{i\frac{\omega x}{c}}\right)$$

$$E_z^p = \frac{4\pi i\omega en}{c^2 kk_p}\left(\frac{\omega}{ck_v} - i\right)e^{k_p x}\,.$$

$$\epsilon = 1 - \omega_p^2/\omega^2 \simeq -\omega_p^2/\omega^2 \qquad \omega_* \simeq min\{\tau^{-1}; c/L\}$$

$$en^e = \lambda\theta(t)(\theta(vt - x) - \theta(vt - c\tau - x))\exp(-z^2/L^2)/(Lv\tau\sqrt{\pi})$$

$\sim 100pC/\mu m$ escaping from the spot with $L \sim 5\mu m$ can generate surface electric field up to TV/m.

$$\boxed{E_x^{sv} = \frac{4\sqrt{\pi}\lambda}{\omega_p \tau L}\left(e^{-\frac{(ct\mp z)^2}{L^2}} - e^{-\frac{(ct - c\tau \mp z)^2}{L^2}}\right)}$$

- surface wave

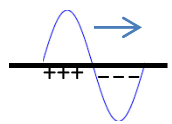

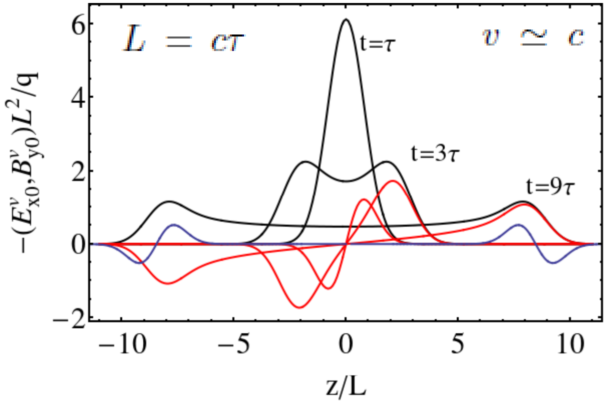

$$j_z^p = \frac{i\lambda\omega_p}{2c\tau}\int\frac{dk}{\pi k}[J_0(ck(t-\tau)) - J_0(ckt)]e^{-\frac{k^2L^2}{4}}e^{ikz + \frac{cx}{\omega_p}}$$

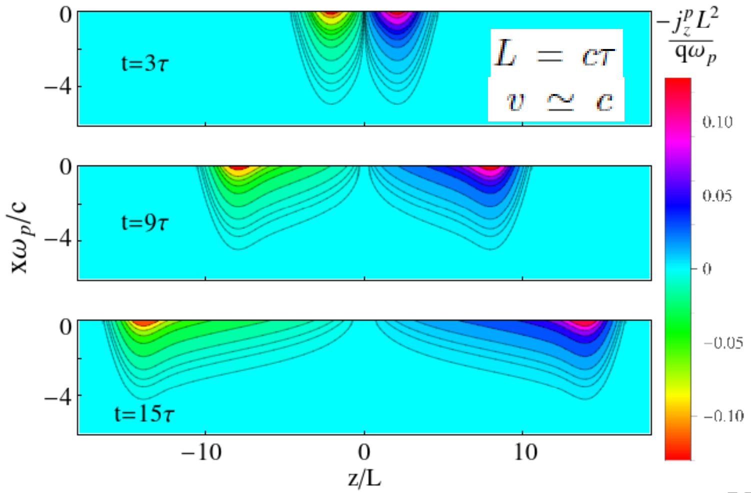

Simulations of the polarization charging

1 FDTD-simulations, $Q_{tot} = 0$

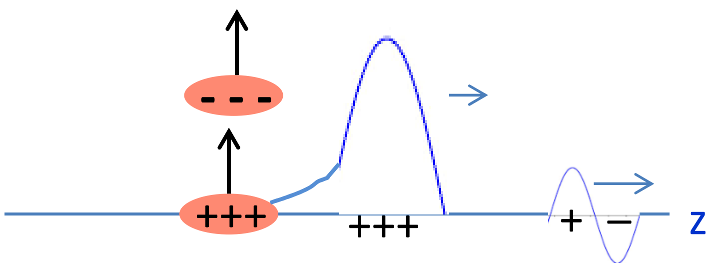

Drude model, $\epsilon = 1 + 4\pi i \sigma(\omega)/\omega$

$$\sigma = \sigma_0/(1 - i\omega/\nu)$$

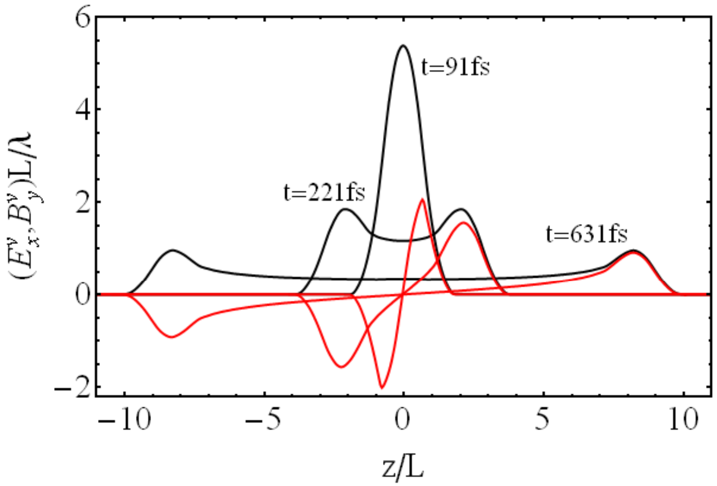

$\sigma_0 = 10^{18}\mathrm{s}^{-1}$ $\nu = 10^{13} 1/\mathrm{s}$

2 2D PIC-simulations

multi-GeV/m field at the distance ~ 1cm

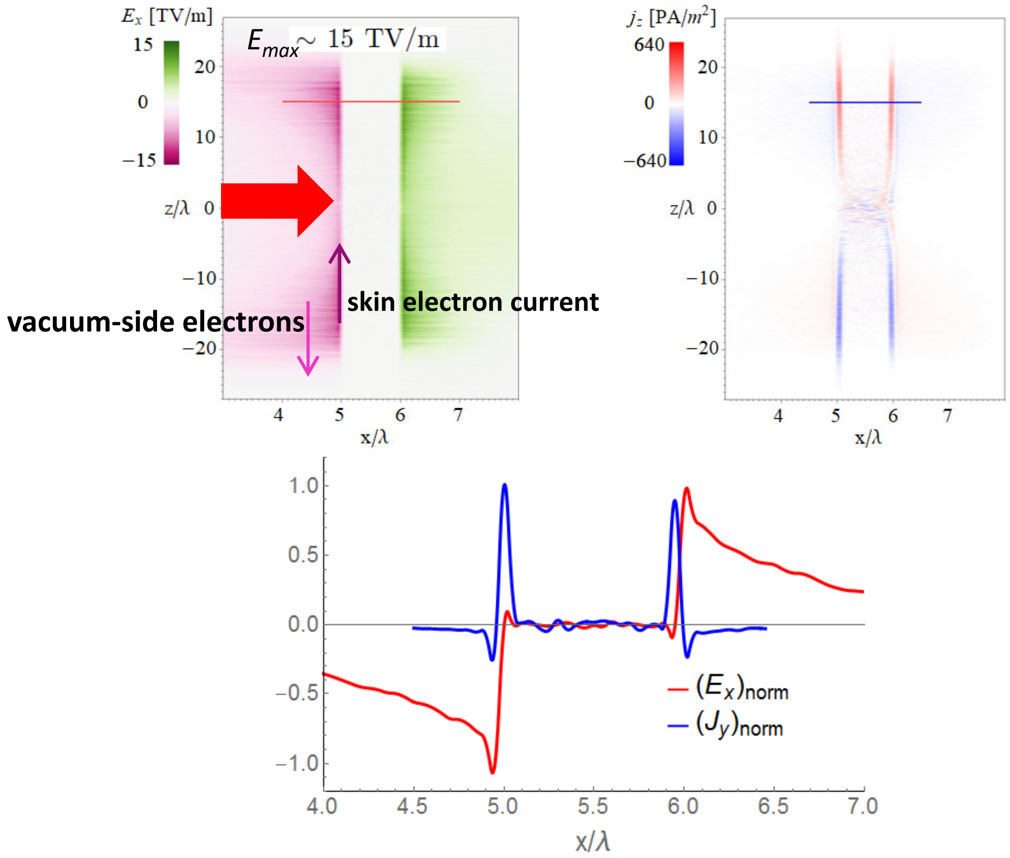

Extreme light diagnostics by ponderomotive acceleration of protons from rarified gas

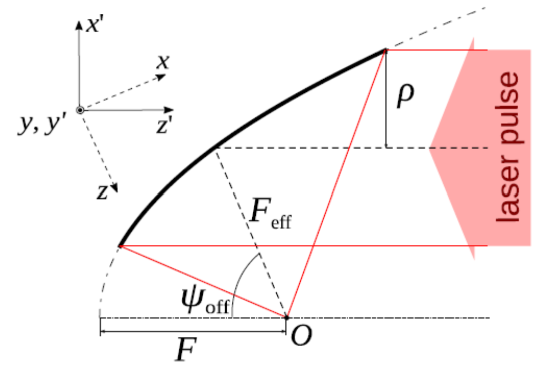

Figure 1. Schematic of laser pulse focused by off-axis parabolic mirror. F, F_{eff} are parent and effective focal lengths, ψ_{off} is the off-axis angle, ρ is the mirror radius.

O. Vais et al., New J. Phys. 22, 023003 (2020).

Focal laser field at the diffraction limit, $D_F \sim \lambda$

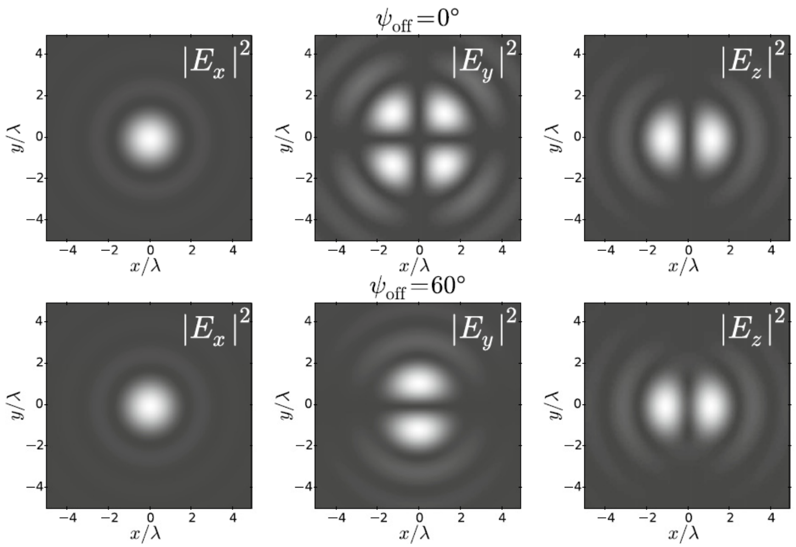

1) $$\frac{\mathrm{d}\gamma\mathbf{v}}{\mathrm{d}t} = \frac{q}{m}\left(\mathbf{E} + \frac{[\mathbf{v}\times\mathbf{B}]}{c}\right), \quad \frac{\mathrm{d}\mathbf{R}}{\mathrm{d}t} = \mathbf{v}$$

2) $$\gamma \simeq 1 \qquad a_{0p} = \frac{a_0}{1840} \qquad a_{0p} \ll 1$$

$$\vec{F}_{\mathrm{p}} = -\frac{q^2}{4m\omega^2}\vec{\nabla}|\vec{E}|^2$$

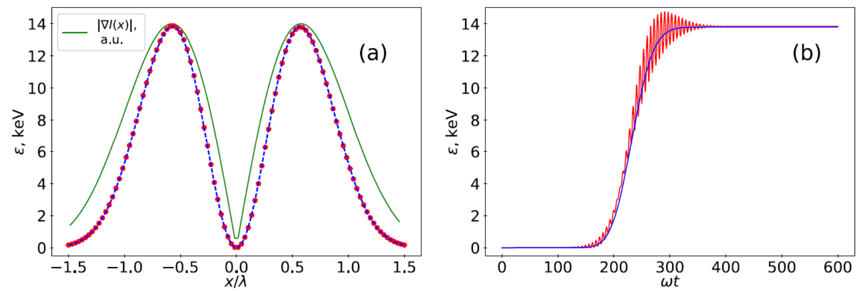

Figure 2. Comparison of results obtained by Lorentz force (red color) and ponderomotive force (blue color): (a) final energy as a function of initial proton position along x-axis ($y = 0, z = 0$) and the absolute value of intensity gradient of Gaussian laser beam (green line), (b) average energy (from the ponderomotive approximation) and its moving average (from Lorentz approach) as a function of time. Numerical calculations were performed for a Gaussian laser pulse with peak intensity $I_p = 10^{22}$ W cm^{-2} and $\tau_{\text{FWHM}} = 36$ fs, focused to a spot of size $D_F = 1.32\lambda$.

Diagnostics: intensity, focusing sharpness

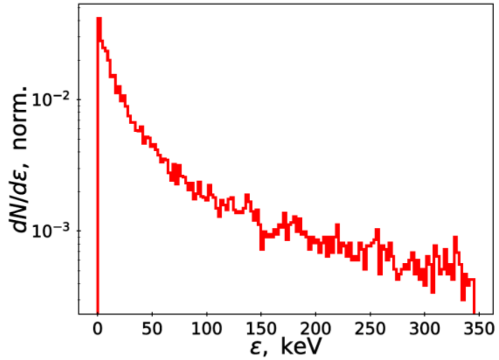

ϑ-integrated spectral distributions of protons accelerated by a Gaussian laser pulse with duration τ=36 fs and peak intensity $I=5\times10^{22}$ W cm^{-2}, focused by an off-axis parabolic mirror (ρ = 5.08 cm, ψ_{off} = 90°) to a focal spot size D_F=1.3λ.

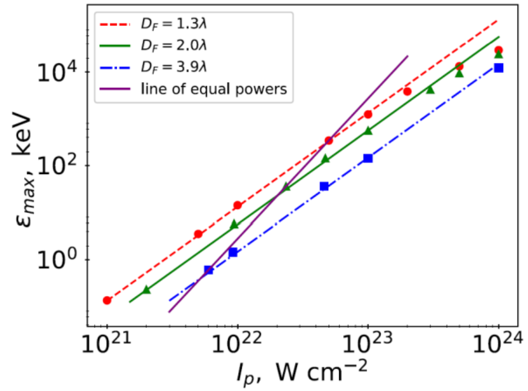

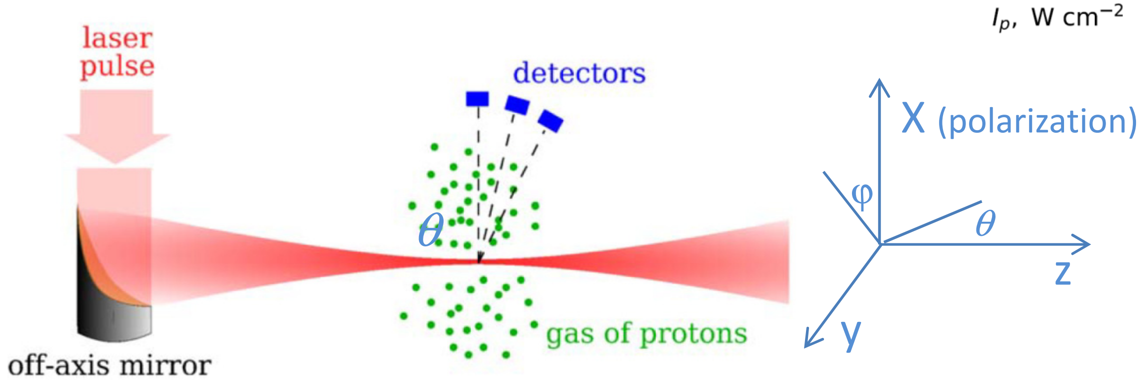

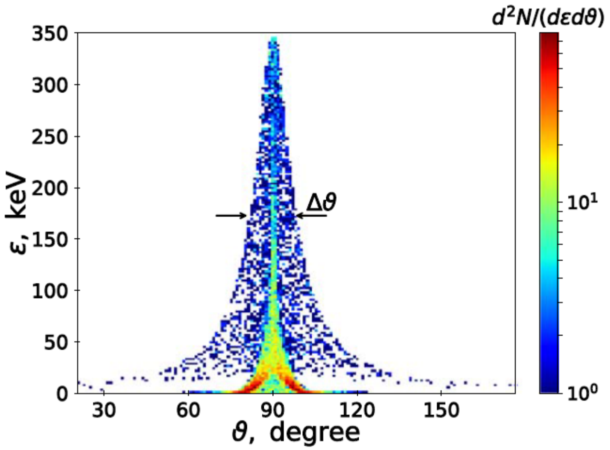

Table 1. Numerically calculated angular width of proton spectra for different values of the focal spot size for the Gaussian laser pulse.

$f_\#$	D_F	z_R	$\Delta\vartheta$, deg.	$\tan(\Delta\vartheta/2)$	$\tan(\Delta\vartheta/2)/(D_F/z_R)$
1	1.3λ	7.8λ	15.4	0.14	0.84
1.5	2.0λ	18λ	9.8	0.086	0.77
3	3.9λ	73.6λ	4.95	0.043	0.81

Diagnostics: pulse duration, spatial focal inhomogeneity

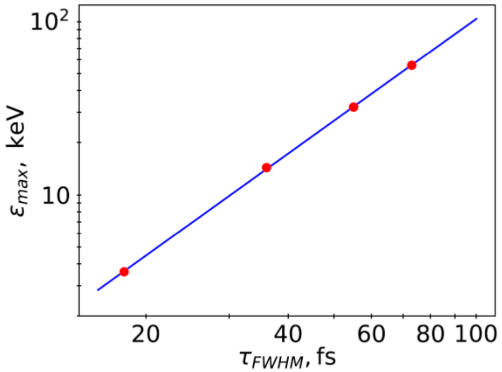

The cutoff energies as a function of the pulse duration τ_{FWHM} of the Gaussian laser pulse with $I=10^{22}$W cm^{-2} and $D_F=1.32\lambda$. Dots show results of numerical calculations, line is a result of the fitting.

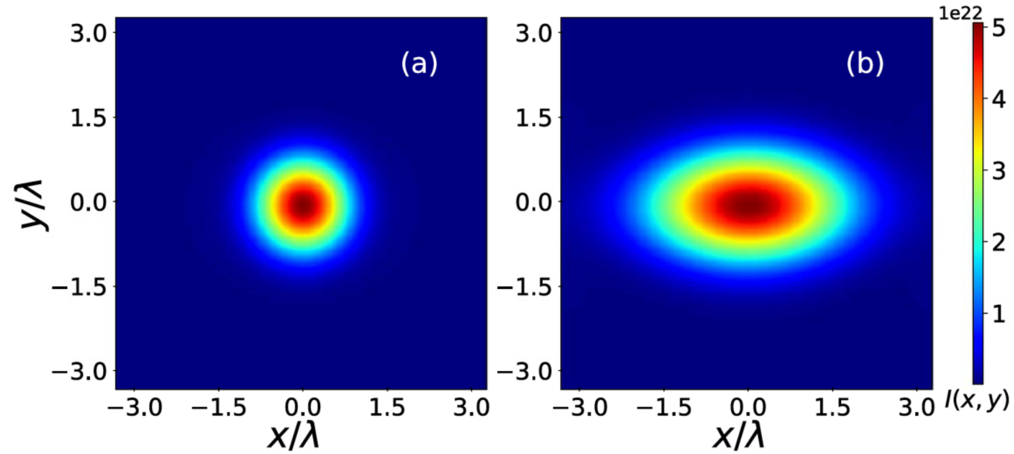

Figure 7. Focal profiles of focused laser pulses with different initial spatial distributions. The laser intensity is measured in W cm^{-2}.

$$\exp(-(x'^2 + y'^2)/w_0^2)$$

$$\exp(-(x'^2 + y'^2)/w_0^2)\Theta(x')$$

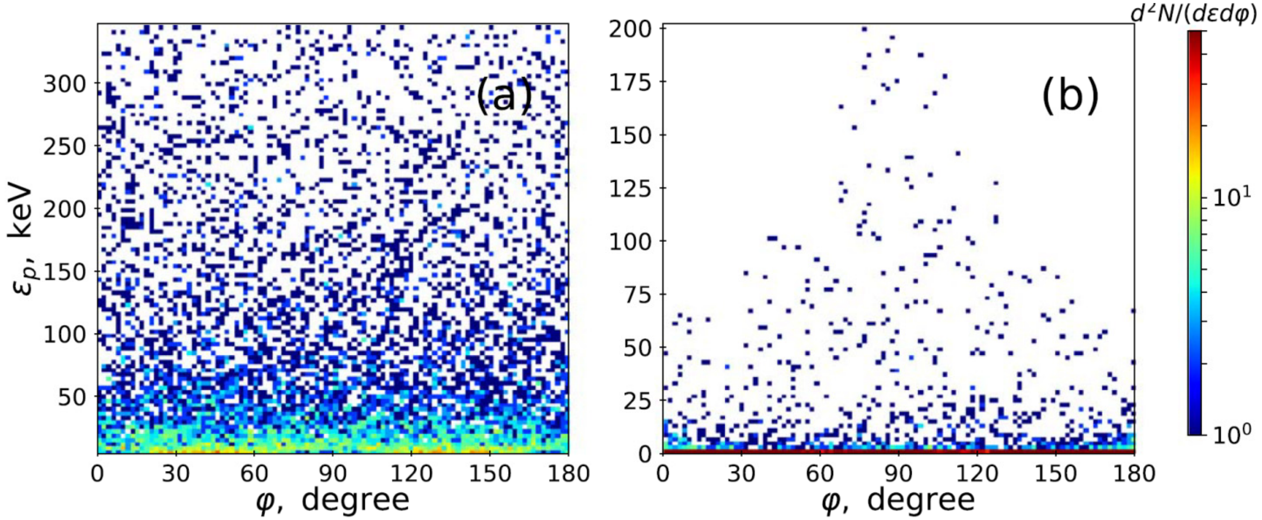

Figure 8. ϑ-integrated spectral distributions of protons accelerated by axial symmetric (a) and anisotropic (b) laser pulses, corresponding to the focal distributions shown in figures 7(a) and (b).

Practical implementation

$N_V > 10^4$

$n_H < 10^{16}$cm^{-3}

chevron type MCP detectors
and/or
nuclear track detectors CR-39

Conclusions

•Electron acceleration in self-trapping regime from low density targets provides maximum total electron charge for relativistic pulses.

•Self-trapping regime makes it useful for production of gammas and photonuclear particles from converter target.

• Betatron emission demonstrates the record yield and photon energy (up to MeV) from self-trapping regime.

•Other nuclear applications can be of interest (fission, transmutation).

• The physics of ultrafast target charging in a wave form due to polarization triggered by laser-accelerated electrons is well clarified and founded.

• Weaker, but still intense, field pulse can propagate along surface (wire) in the form of surface (Sommerfeld) wave for a long distance.

• Innovative diagnostics of ultra-intense laser pulses through ion acceleration is proposed.

Thank you